The Astrophysical Journal, 754:145 (17pp), 2012 August 1 doi:10.1088/0004-637X/754/2/145
© 2012. The American Astronomical Society. All rights reserved. Printed in the U.S.A.

LOCALIZING *INTEGRAL* SOURCES WITH *CHANDRA*: X-RAY AND MULTI-WAVELENGTH IDENTIFICATIONS AND ENERGY SPECTRA

John A. Tomsick[1], Arash Bodaghee[1], Sylvain Chaty[2,3], Jerome Rodriguez[2], Farid Rahoui[4,5], Jules Halpern[6], Emrah Kalemci[7], and Mehtap Özbey Arabaci[8]
[1] Space Sciences Laboratory, 7 Gauss Way, University of California, Berkeley, CA 94720-7450, USA; jtomsick@ssl.berkeley.edu
[2] AIM (UMR-E 9005 CEA/DSM-CNRS-Université Paris Diderot) Irfu/Service d'Astrophysique, Centre de Saclay, FR-91191 Gif-sur-Yvette Cedex, France
[3] Institut Universitaire de France, 103 bd Saint-Michel, 75005 Paris, France
[4] Astronomy Department, Harvard University, 60 Garden Street, Cambridge, MA 02138, USA
[5] Harvard-Smithsonian Center for Astrophysics, 60 Garden Street, Cambridge, MA 02138, USA
[6] Columbia Astrophysics Laboratory, Columbia University, 550 West 120th Street, New York, NY 10027-6601, USA
[7] Faculty of Engineering and Natural Sciences, Sabancı University, Orhanlı-Tuzla, İstanbul 34956, Turkey
[8] Physics Department, Middle East Technical University, Ankara 06531, Turkey
Received 2012 April 5; accepted 2012 June 4; published 2012 July 18

ABSTRACT

We report on *Chandra* observations of 18 hard X-ray (>20 keV) sources discovered with the *INTEGRAL* satellite near the Galactic plane. For 14 of the *INTEGRAL* sources, we have uncovered one or two potential *Chandra* counterparts per source. These provide soft X-ray (0.3–10 keV) spectra and subarcsecond localizations, which we use to identify counterparts at other wavelengths, providing information about the nature of each source. Despite the fact that all of the sources are within 5° of the plane, four of the IGR sources are active galactic nuclei (AGNs; IGR J01545+6437, IGR J15391–5307, IGR J15415–5029, and IGR J21565+5948) and four others are likely AGNs (IGR J03103+5706, IGR J09189–4418, IGR J16413–4046, and IGR J16560–4958) based on each of them having a strong IR excess and/or extended optical or near-IR emission. We compare the X-ray and near-IR fluxes of this group of sources to those of AGNs selected by their 2–10 keV emission in previous studies and find that these IGR AGNs are in the range of typical values. There is evidence in favor of four of the sources being Galactic (IGR J12489–6243, IGR J15293–5609, IGR J16173–5023, and IGR J16206–5253), but only IGR J15293–5609 is confirmed as a Galactic source as it has a unique *Chandra* counterpart and a parallax measurement from previous optical observations that puts its distance at 1.56 ± 0.12 kpc. The 0.3–10 keV luminosity for this source is $(1.4^{+1.0}_{-0.4}) \times 10^{32}$ erg s^{-1}, and its optical/IR spectral energy distribution is well described by a blackbody with a temperature of 4200–7000 K and a radius of 12.0–16.4 $R_{\odot}$. These values suggest that IGR J15293–5609 is a symbiotic binary with an early K-type giant and a white dwarf accretor. We also obtained likely *Chandra* identifications for IGR J13402–6428 and IGR J15368–5102, but follow-up observations are required to constrain their source types.

Key words: galaxies: active – stars: individual (IGR J01545+6437, IGR J03103+5706, IGR J04069+5042, IGR J06552–1146, IGR J09189–4418, IGR J12489–6243, IGR J13402–6428, IGR J15293–5609, IGR J15368–5102, IGR J15391–5307, IGR J15415–5029, IGR J16173–5023, IGR J16206–5253, IGR J16413–4046, IGR J16560–4958, IGR J21188+4901) – stars: neutron – white dwarfs – X-rays: galaxies – X-rays: stars

1. INTRODUCTION

The hard X-ray imaging of the Galactic plane by the *INTErnational Gamma-Ray Astrophysics Laboratory* (*INTEGRAL*) satellite continues to find new "IGR" sources at energies >20 keV. While *INTEGRAL* excels at discovering new sources in the 20–40 keV band, especially due to its large field of view (FOV), it only localizes them to 1′–5′, which is not nearly adequate for finding optical/IR counterparts. Short *Chandra* exposures of IGR sources allow for a major advance in understanding the nature of these sources by providing subarcsecond positions, leading to unique optical/IR counterparts, as well as 0.3–10 keV spectra that can be used to measure column densities and continuum shapes.

After observations between 2003 and 2008, *INTEGRAL* had detected more than 700 hard X-ray sources (Bird et al. 2010). While that catalog includes nearly 400 IGR sources, the most up-to-date list[9] includes more than 500 IGR entries. The largest group of identified sources are the active galactic nuclei (AGNs) with >250 confirmed AGNs detected (Bird et al. 2010). The largest Galactic source types include high-mass X-ray binaries (HMXBs), low-mass X-ray binaries (LMXBs), and cataclysmic variables (CVs). A subset of these binaries are symbiotics with a white dwarf or neutron star accreting from a giant (i.e., luminosity class III) star. It has been somewhat surprising that the symbiotics with white dwarf accretors can produce hard X-ray emission (Kennea et al. 2009; Ratti et al. 2010). In addition, *INTEGRAL* has detected new as well as known supernova remnants and pulsar wind nebulae. Unidentified IGR sources are also still a large group, and the most critical piece of information for determining the nature of these sources is to obtain a subarcsecond X-ray position.

Even the faintest *INTEGRAL* detections, which are near $\sim 2 \times 10^{-12}$ erg cm^{-2} s^{-1} (20–40 keV), are usually easily detected by *Chandra* in a short exposure time. With our previous *Chandra* programs, we obtained 5 ks snapshots of 46 IGR sources, and obtained 35 *Chandra* counterparts (Tomsick et al. 2006, 2008, 2009). Based on *Chandra* spectral information and optical/IR observations (e.g., Masetti et al. 2009; Chaty et al. 2008; Butler et al. 2009), definite or likely identifications have been obtained for 32 of our *Chandra* targets. These programs have all concentrated on low Galactic latitude targets

[9] See http://irfu.cea.fr/Sap/IGR-Sources/.

Table 1
Chandra Observations

IGR Name	ObsID	l^a	b^b	Start Time	Exposure Time (s)
J01545+6437	12425	129.62	+2.57	2011 Feb 7, 19.47 h UT	4987
J03103+5706	12419	140.95	−0.83	2010 Nov 23, 10.39 h UT	4716
J04069+5042	12421	151.43	−1.03	2010 Nov 25, 5.47 h UT	4987
J06552–1146	12433	223.85	−4.52	2010 Dec 12, 22.35 h UT	4986
J09189–4418	12426	267.93	+3.64	2011 Jul 22, 0.37 h UT	5007
J12489–6243	12416	302.64	+0.15	2010 Nov 25, 22.19 h UT	4986
J13402–6428	12424	308.15	−2.10	2011 Oct 6, 9.38 h UT	4995
J15293–5609	12417	323.66	+0.22	2011 Jun 22, 22.08 h UT	5096
J15368–5102	12428	327.52	+3.76	2011 Oct 9, 2.91 h UT	4695
J15391–5307	12422	326.58	+1.88	2011 Apr 14, 21.18 h UT	4992
J15415–5029	12429	328.45	+3.76	2011 Oct 9, 1.13 h UT	4994
J16173–5023	12415	332.84	+0.14	2011 Oct 11, 5.28 h UT	4989
J16206–5253	12423	331.47	−2.01	2011 Jul 5, 18.10 h UT	4992
J16413–4046	12427	342.71	+3.70	2011 May 9, 0.50 h UT	4991
J16560–4958	12431	337.32	−4.17	2011 May 23, 5.91 h UT	4992
J21188+4901	12418	91.27	−0.33	2011 Feb 28, 2.77 h UT	4989
J21565+5948	12430	102.54	+4.06	2011 May 30, 20.79 h UT	4992
J22014+6034	12432	103.49	+4.28	2011 Apr 16, 11.82 h UT	4994

Notes.
[a] Galactic longitude in degrees measured by *INTEGRAL*.
[b] Galactic latitude in degrees measured by *INTEGRAL*.

as the *Chandra* positions are most critical for obtaining optical and IR counterparts in the crowded regions of the Galactic plane. Although our scientific goals have leaned toward finding Galactic sources such as obscured HMXBs (Matt & Guainazzi 2003; Filliatre & Chaty 2004; Walter et al. 2006; Chaty & Rahoui 2012) or supergiant fast X-ray transients (SFXTs; Negueruela et al. 2006; Smith et al. 2006; Pellizza et al. 2006), it has still been relatively common to find that the *INTEGRAL* sources are background AGNs (e.g., Zurita Heras et al. 2009).

In the following, we describe the results of *Chandra* observations of 18 IGR sources that were made between late-2010 and late-2011. The observations are described in Section 2, and the search for X-ray counterparts, fits to the *Chandra* energy spectra, and multi-wavelength identifications are described in Section 3. A discussion of the results for each source is provided in Section 4, and Section 5 includes a summary.

2. *CHANDRA* OBSERVATIONS AND DATA PROCESSING

When the target selection was done for this program, we considered 723 sources listed in the fourth *INTEGRAL* survey catalog of Bird et al. (2010). We excluded sources if their classification (e.g., AGN, HMXB, etc.) was known according to Bird et al. (2010) or the *INTEGRAL* sources Web site[9], and we only considered sources situated within 5° of the Galactic plane. From 98 low-latitude sources, we removed sources labeled as transient in Bird et al. (2010), as well as sources with previous or planned observations by *Chandra*, *XMM-Newton*, or *Swift*.

After the selections described above, we were left with 19 sources that we observed with *Chandra*. We reported on one target, IGR J11014–6103, in a separate paper (Tomsick et al. 2012) and the other 18 targets here. Table 1 lists the sources, their *INTEGRAL* positions, and basic information about the *Chandra* observations. The observations of the IGR source fields occurred between 2010 November 23 and 2011 October 11, and, in each case, an exposure time of ∼5 ks was obtained. We used the Advanced CCD Imaging Spectrometer (ACIS; Garmire et al. 2003) instrument, which has a 0.3–10 keV bandpass. The 90% confidence *INTEGRAL* error circles range from 3.′3 to 5.′4, leading us to use the 16.9 × 16.9 arcmin^2 FOV of the ACIS-I instrument. We used the ACIS "Faint" mode because of the potential for bright sources to saturate the *Chandra* telemetry if we used "Very Faint" mode. In addition, we used a custom dither pattern to decrease the non-uniformity of the exposure time due to gaps between the four ACIS-I chips.

The data were initially processed at the Chandra X-ray Center (CXC) with ASCDS versions between 8.3.3.1 and 8.4. After obtaining the data from the CXC, we performed all subsequent processing with the *Chandra* Interactive Analysis of Observations (CIAO) version 4.3.1 software and Calibration Database version 4.4.6. We used the CIAO program `chandra_repro` to produce the "level 2" event lists that we used for further analysis.

3. ANALYSIS AND GENERAL RESULTS

3.1. Search for X-ray Counterparts to the IGR Sources

We used the CIAO routine `wavdetect` to search for X-ray sources on the ACIS-I chips. For each observation, we searched for sources in unbinned images with 2048 × 2048 pixels as well as images binned by a factor of two (1024 × 1024 pixels), a factor of four (512 × 512 pixels), and a factor of eight (256 × 256 pixels). In each case, we set the detection threshold to a level that would be expected to yield one spurious source (2.4×10^{-7}, 9.5×10^{-7}, 3.8×10^{-6}, and 1.5×10^{-5}, respectively, corresponding to the inverse of the number of pixels for each of the four images). Thus, in the merged lists of detected sources, it would not be surprising if a few of the sources in each field are spurious.

Although we typically detected dozens of *Chandra* sources in each field, we used information about their brightnesses, their hardnesses, and their locations relative to the *INTEGRAL* error circle to determine which sources to consider as candidate counterparts to the *INTEGRAL* sources. To determine the most likely candidates, we followed the technique used in Tomsick et al. (2009). The broadest Galactic plane survey to date that resulted in a suitable log N– log S curve was obtained with the *Advanced Satellite for Cosmology and Astrophysics* (*ASCA*).

Table 2
Chandra Candidate Counterparts to IGR Sources

IGR Name	CXOU Name	$\theta^{a}/\theta_{\rm INTEGRAL}{}^{b}$ (arcminutes)	*Chandra* R.A.[c] (J2000)	*Chandra* Decl.[c] (J2000)	ACIS Counts[d]	Hardness[e]
J01545+6437	J015435.2+643757 (1)	1.32/4.1	$01^{h}54^{m}35\overset{s}{.}28$	$+64^{\circ}37'57\overset{''}{.}8$	29.3	$+0.40 \pm 0.26$
J03103+5706	J031010.6+570712 (2)	1.37/4.9	$03^{h}10^{m}10\overset{s}{.}61$	$+57^{\circ}07'12\overset{''}{.}1$	17.4	$+0.79 \pm 0.41$
J09189–4418	J091858.8–441830 (3)	0.64/4.5	$09^{h}18^{m}58\overset{s}{.}83$	$-44^{\circ}18'30\overset{''}{.}9$	377.4	$+0.79 \pm 0.07$
J12489–6243	J124846.4–623743 (4a)	5.42/4.1	$12^{h}48^{m}46\overset{s}{.}44$	$-62^{\circ}37'43\overset{''}{.}1$	38.1	$+0.67 \pm 0.24$
	J124905.3–624242 (4b)	1.40/4.1	$12^{h}49^{m}05\overset{s}{.}32$	$-62^{\circ}42'42\overset{''}{.}6$	16.3	$+0.16 \pm 0.35$
J13402–6428	J133935.8–642537 (5a)	5.02/3.5	$13^{h}39^{m}35\overset{s}{.}89$	$-64^{\circ}25'37\overset{''}{.}7$	97.7	$+0.38 \pm 0.13$
	J133959.2–642444 (5b)	4.29/3.5	$13^{h}39^{m}59\overset{s}{.}25$	$-64^{\circ}24'44\overset{''}{.}3$	31.7	$+0.16 \pm 0.24$
J15293–5609	J152929.3–561213 (6)	3.08/5.4	$15^{h}29^{m}29\overset{s}{.}37$	$-56^{\circ}12'13\overset{''}{.}3$	119.4	-0.51 ± 0.12
J15368–5102	J153658.6–510221 (7)	1.82/4.9	$15^{h}36^{m}58\overset{s}{.}64$	$-51^{\circ}02'21\overset{''}{.}4$	77.4	$+0.23 \pm 0.14$
J15391–5307	J153916.7–530815 (8)	2.25/4.5	$15^{h}39^{m}16\overset{s}{.}78$	$-53^{\circ}08'15\overset{''}{.}9$	46.5	$+1.01 \pm 0.25$
J15415–5029	J154126.4–502823 (9a)	1.12/3.8	$15^{h}41^{m}26\overset{s}{.}45$	$-50^{\circ}28'23\overset{''}{.}5$	46.4	$+0.71 \pm 0.22$
	J154140.5–502848 (9b)	2.02/3.8	$15^{h}41^{m}40\overset{s}{.}57$	$-50^{\circ}28'48\overset{''}{.}6$	15.4	$+0.11 \pm 0.37$
J16173–5023	J161728.2–502242 (10a)	2.11/3.3	$16^{h}17^{m}28\overset{s}{.}26$	$-50^{\circ}22'42\overset{''}{.}5$	694.6	$+0.36 \pm 0.04$
	J161720.6–502415 (10b)	1.38/3.3	$16^{h}17^{m}20\overset{s}{.}65$	$-50^{\circ}24'15\overset{''}{.}1$	15.4	$+1.02 \pm 0.49$
J16206–5253	J161955.4–525230 (11)	6.09/4.6	$16^{h}19^{m}55\overset{s}{.}49$	$-52^{\circ}52'30\overset{''}{.}2$	70.3	$+0.80 \pm 0.18$
J16413–4046	J164119.4–404737 (12)	0.81/4.5	$16^{h}41^{m}19\overset{s}{.}49$	$-40^{\circ}47'37\overset{''}{.}7$	147.4	$+0.91 \pm 0.12$
J16560–4958	J165551.9–495732 (13)	0.99/4.1	$16^{h}55^{m}51\overset{s}{.}95$	$-49^{\circ}57'32\overset{''}{.}4$	1092.4	$+0.54 \pm 0.04$
J21565+5948	J215604.2+595604 (14)	7.88/4.9	$21^{h}56^{m}04\overset{s}{.}22$	$+59^{\circ}56'04\overset{''}{.}1$	202.8	$+0.11 \pm 0.08$

Notes.
[a] The angular distance between the center of the *INTEGRAL* error circle, which is also the approximate *Chandra* aimpoint, and the source.
[b] The size of the 90% confidence *INTEGRAL* error radius given in Bird et al. (2010).
[c] The position uncertainties for these relatively bright sources are dominated by the systematic error, which is $0\overset{''}{.}64$ at 90% confidence and $1''$ at 99% confidence (Weisskopf 2005).
[d] The number of counts, after background subtraction, measured by *Chandra*/ACIS-I in the 0.3–10 keV band.
[e] The hardness is given by $(C_2 - C_1)/(C_2 + C_1)$, where C_2 is the number of counts in the 2–10 keV band and C_1 is the number of counts in the 0.3–2 keV band.

The 2–10 keV $\log N - \log S$ is described as a power law with $N(>F_{2-10\,\rm keV}) = 9.2(F_{2-10\,\rm keV}/10^{-13})^{-0.79}$ deg^{-2}, where $F_{2-10\,\rm keV}$ is the absorbed 2–10 keV flux in units of erg cm^{-2} s^{-1} (Sugizaki et al. 2001). Although this relationship is meant to be for Galactic sources only, Sugizaki et al. (2001) as well as Hands et al. (2004), which combines the *ASCA* measurements with *Chandra* and *XMM-Newton* $\log N - \log S$ measurements for smaller regions of the plane, suggest that the above relationship is a good approximation to the total source density down to a flux level of a few $\times 10^{-13}$ erg cm^{-2} s^{-1}. Thus, we use this relationship for our initial calculations, but we discuss the impact of a steeper $\log N - \log S$ on our faintest *Chandra* candidates in Section 3.3. Using Poisson statistics, the probability (P) that a source is spurious is given by

$$P = 1 - e^{-N(>F_{2-10\,\rm keV})\pi\theta^{2}_{\rm search}}, \quad (1)$$

where $\theta_{\rm search}$ is the radius of the search region in units of degrees. In cases where a source is within the 90% confidence *INTEGRAL* error circle, which has a radius of $\theta_{\rm INTEGRAL}$, the error circle is the search region (i.e., $\theta_{\rm search} = \theta_{\rm INTEGRAL}$). For sources outside the error circle, $\theta_{\rm search} = \theta$, where θ is the angular separation between the source and the center of the *INTEGRAL* error circle.

While calculating the absolute spurious probabilities requires spectral modeling to determine source fluxes, here, we calculate a relative probability, $P_{\rm rel}$, using the 2–10 keV count rates, $C_{2-10\,\rm keV}$ according to

$$P_{\rm rel} = 1 - e^{-(\frac{C_{2-10\,\rm keV}}{C_0})^{-0.79}\pi\theta^{2}_{\rm search}}, \quad (2)$$

where C_0 is an arbitrary number of counts. We set this parameter to 520, which makes the source with the highest number of counts in the 2–10 keV band have $P_{\rm rel} = 0.01$.

After carrying out the spectral analysis (Section 3.2) and determining the actual fluxes for a subset of the sources, we find that a value of $P_{\rm rel} = 0.3$ corresponds to a 10%–25% spurious probability, where the large range is caused by the variation in the counts-to-flux ratio with the hardness of the spectrum. We consider $P_{\rm rel} = 0.3$ to be our threshold for further consideration of a source as a candidate counterpart. We made only two exceptions to the strict threshold: for IGR J09189–4418, we do not consider two candidates with $P_{\rm rel} = 0.29$ because there is a much better candidate with $P_{\rm rel} = 0.02$, and for IGR J16413–4046, we do not consider a candidate that is right at the threshold because there is a candidate with $P_{\rm rel} = 0.05$.

With these criteria, we find four cases with no *Chandra* sources that stand out from the general X-ray source population: IGR J04069+5042, IGR J06552–1146, IGR J21188+4901, and IGR J22014+6034, and for these sources, we include lists of detected sources in these fields in the Appendix. Ten sources have unique candidate counterparts, and four sources have two candidate counterparts. The final list of 18 sources that we consider as potential or likely counterparts to the IGR sources is given in Table 2. For IGR sources with two *Chandra* counterparts, the first source is the one with lower $P_{\rm rel}$.

The hardness–intensity diagram, including all of the detected *Chandra* sources, is shown in Figure 1. For each source, we determined the number of source counts in the 0.3–2 keV band (C_1) and the 2–10 keV band (C_2). Using the size of the *Chandra*

point-spread function (PSF) as a guide, we used extraction radii of 5″ for sources within 4′ of the aimpoint, 10″ for sources between 4′ and 7′ from the aimpoint, and 15″ for sources more than 7′ from the aimpoint. The background counts were taken from a rectangular source-free region, scaled to the size of the source extraction region, and subtracted off. We then calculated the hardness according to $(C_2 - C_1)/(C_2 + C_1)$, which runs from –1.0 for the softest sources (all the counts in the 0.3–2 keV band) to +1.0 for the hardest sources (all the counts in the 2–10 keV band). To deal with the case where there are zero counts in one of the energy bands, we used the "Gehrels" prescription for determining the uncertainties (Gehrels 1986). The sources that we are considering as candidate counterparts are labeled, and they primarily occupy the region of the diagram with harder and brighter sources. For these sources, the numbers of source counts and the hardnesses are given in Table 2.

3.2. Energy Spectra of the Candidate Counterparts

For each of the candidate counterparts, we produced and modeled the 0.3–10 keV *Chandra* energy spectrum. We extracted source photons from circular regions with radii as described above. Although background is negligible in most cases, we made a background estimate using the rectangular regions described above, and performed background subtraction. We fitted the spectra using the XSPEC v12.7.0 software package. For 16 of the 18 spectra, we fitted unbinned spectra and optimized the fit using Cash statistics.[10] In two cases, the count rates were high enough to cause photon pile-up, and we used χ^2 statistics in these cases. We accounted for pile-up in the two cases using the XSPEC model `pileup` (Davis 2001).

We fitted the spectra with a model consisting of an absorbed power law and used Wilms et al. (2000) abundances and Balucinska-Church & McCammon (1992) cross sections to model the absorption, and the results are shown in Table 3. For each source, the measured column density potentially includes contributions from the Galactic interstellar medium (ISM) as well as from absorption that is intrinsic to the source. The value of $N_{\rm H}$ given in Table 3 is the total, but we also include the Galactic $N_{\rm H}$ from Kalberla et al. (2005) for comparison. For the spectra fitted with Cash statistics, we used the XSPEC routine `goodness` to determine the percentage of simulated spectra with a fit statistic less than that obtained for the data. One expects a value near 50% if the model is consistent with the spectrum, and we obtain an average value of 55%. The values range from 28.6% to 81.4% with three sources having values >75%. For these three cases, we produced binned spectra with at least 10 counts per bin, performed a χ^2 minimization fit, and inspected the residuals. For CXOU J091858.8–441830 and CXOU J215604.2+595604, we obtained reduced-χ^2 (χ^2_ν) values of 1.0 (33 dof) and 0.85 (17 dof), respectively, and there are no obvious features in the residuals in either case. For CXOU J164119.4–404737, $\chi^2_\nu = 1.2$ (12 dof), and there are positive residuals near 5 keV. Adding a Gaussian with an energy of 5.0 ± 0.3 keV provides a marginally significant improvement in the fit to $\chi^2_\nu = 0.95$ (9 dof). It is possible that the source is a background AGN and that the Gaussian is a redshifted iron line. The line energy implies a redshift of $z = 0.28 \pm 0.08$. As the detection of this emission line is marginal, we report the fit parameters with and without the line in Table 3.

[10] Although we follow the XSPEC terminology by calling this the "Cash" statistic, when background subtraction is performed, it is technically the *W*-statistic that is minimized. See http://heasarc.nasa.gov/xanadu/xspec/manual/XSappendixStatistics.html.

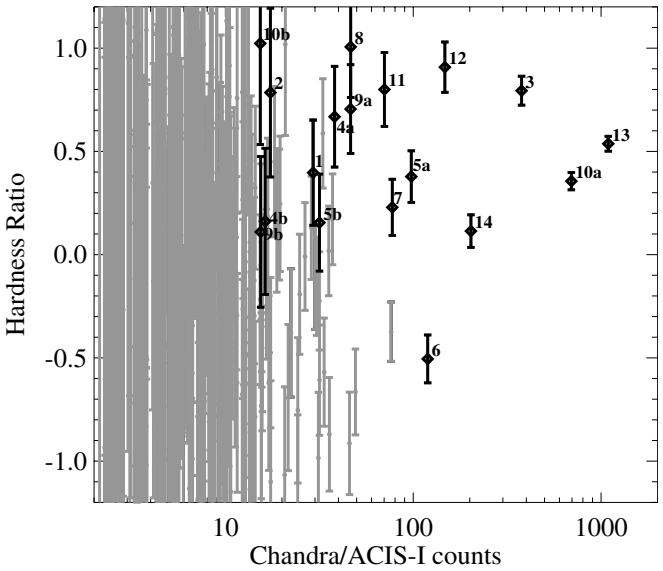

Figure 1. Hardness–intensity diagram, including all of the *Chandra*/ACIS-I sources detected in the 18 *Chandra* observations. The intensity is given as the number of ACIS-I counts in the 0.3–10 keV energy band. The hardness is given by $(C_2 - C_1)/(C_2 + C_1)$, where C_2 is the number of counts in the 2–10 keV band and C_1 is the number of counts in the 0.3–2 keV band. The sources that we consider as possible *Chandra* counterparts to the IGR sources are plotted with black diamonds and error bars. The labels correspond to the sources as follows: 1, IGR J01545+6437; 2, IGR J03103+5706; 3, IGR J09189–4418; 4a, IGR J12489–6243 (candidate a); 4b, IGR J12489–6243 (candidate b); 5a, IGR J13402–6428 (candidate a); 5b, IGR J13402–6428 (candidate b); 6, IGR J15293–5609; 7, IGR J15368–5102; 8, IGR J15391–5307; 9a, IGR J15415–5029 (candidate a); 9b, IGR J15415–5029 (candidate b); 10a, IGR J16173–5023 (candidate a); 10b, IGR J16173–5023 (candidate b); 11, IGR J16206–5253; 12, IGR J16413–4046; 13, IGR J16560–4958; and 14, IGR J21565+5948.

The two candidates with the highest count rates, CXOU J161728.2–502242 and CXOU J165551.9–495732, have spectra that show evidence for photon pile-up. When their spectra, binned with at least 20 counts per bin, are fitted with absorbed power-law models and no pile-up correction, the χ^2_ν values obtained are both 1.8 (31 and 50 dof, respectively). For the former source, a pile-up correction improves the fit to $\chi^2_\nu = 1.32$ (30 dof), but residuals are still seen between 6 and 7 keV. We added a Gaussian emission line with an energy of $6.8^{+0.5}_{-0.4}$ keV, and the fit improves further to $\chi^2_\nu = 1.21$ (27 dof). While the statistical significance of this line is also marginal, we report the fit parameters with the line in Table 3. For CXOU J165551.9–495732, the fit improves to $\chi^2_\nu = 1.1$ (49 dof) with the pile-up correction, and the residuals do not suggest that other spectral components are required.

3.3. Assessing the Likelihood that the Candidate Counterparts Are the True Counterparts of the IGR Sources

With the spectral fits completed, we used Equation (1) to estimate the probabilities of spurious associations between the *Chandra* sources listed in Tables 2 and 3 and their respective IGR sources. We used the spectral parameters given in Table 3 to determine the absorbed 2–10 keV flux for each source. These fluxes are given in Table 4 along with $N(>F_{2-10\,\rm keV})$ (the density of sources on the sky from Sugizaki et al. 2001), θ, $\theta_{\rm INTEGRAL}$, and an estimate of the probability that each association is spurious. Taken as a group of 18 candidates, we would expect probabilities of 5.6%, 11.1%, and 22.2% to correspond to one, two, and four (out of 18) spurious associations. The calculated

Table 3
Chandra Spectral Results

IGR Name	CXOU Name	N_H ($\times 10^{22}$ cm^{-2})	Γ	X-Ray Flux[a]	α[b]	Fit Statistic[c]	Galactic N_H ($\times 10^{22}$ cm^{-2})[d]
J01545+6437	J015435.2+643757 (1)	$0.0^{+0.4}_{-0.0}$	$-0.40^{+0.56}_{-0.59}$	$0.30^{+0.16}_{-0.11}$	...	177.4/660 (54.6%)	0.67
J03103+5706	J031010.6+570712 (2)	$4.5^{+15.5}_{-3.7}$	$2.2^{+5.1}_{-1.8}$	$0.9^{+90,000}_{-0.6}$	...	109.7/660 (43.2%)	0.74
J09189–4418	J091858.8–441830 (3)	$4.6^{+1.1}_{-1.3}$	$1.4^{+0.4}_{-0.4}$	$4.1^{+1.5}_{-0.7}$	...	534.2/660 (80.3%)	0.43
J12489–6243	J124846.4–623743 (4a)	$0.0^{+1.2}_{-0.0}$	$-0.83^{+0.76}_{-0.56}$	$0.54^{+0.25}_{-0.11}$	...	205.9/660 (28.6%)	1.28
	J124905.3–624242 (4b)	$4.2^{+5.3}_{-2.9}$	$3.5^{+2.7}_{-1.9}$	$1.3^{+400}_{-1.2}$	...	103.1/660 (65.1%)	1.37
J13402–6428	J133935.8–642537 (5a)	$1.2^{+0.9}_{-0.8}$	1.0 ± 0.6	$0.71^{+0.16}_{-0.14}$	...	314.0/660 (29.5%)	1.02
	J133959.2–642444 (5b)	$1.7^{+2.4}_{-1.4}$	$1.9^{+1.5}_{-1.1}$	$0.27^{+1.39}_{-0.12}$	...	171.9/660 (60.9%)	1.03
J15293–5609	J152929.3–561213 (6)	$0.34^{+0.28}_{-0.23}$	$2.4^{+0.6}_{-0.5}$	$0.47^{+0.34}_{-0.13}$	...	249.8/660 (56.4%)	1.56
J15368–5102	J153658.6–510221 (7)	$0.84^{+0.82}_{-0.61}$	1.3 ± 0.6	$0.44^{+0.14}_{-0.10}$	...	269.6/660 (41.7%)	0.40
J15391–5307	J153916.7–530815 (8)	37^{+29}_{-19}	$3.2^{+3.0}_{-2.1}$	$52^{+150,000}_{-50}$	...	194.7/660 (49.4%)	0.96
J15415–5029	J154126.4–502823 (9a)	$0.0^{+1.1}_{-0.0}$	$-0.43^{+0.68}_{-0.44}$	$0.56^{+0.21}_{-0.17}$	...	235.7/660 (55.5%)	0.44
	J154140.5–502848 (9b)	$0.5^{+1.6}_{-0.5}$	$1.3^{+1.5}_{-1.0}$	$0.07^{+0.13}_{-0.03}$	...	101.3/660 (49.5%)	0.45
J16173–5023	J161728.2–502242 (10a)[e]	$0.57^{+0.31}_{-0.25}$	$0.97^{+0.34}_{-0.30}$	$6.1^{+2.8}_{-1.5}$	$0.34^{+0.38}_{-0.23}$	32.7/27	1.94
	J161720.6–502415 (10b)	22^{+39}_{-19}	$1.4^{+4.1}_{-2.7}$	$1.5^{+33}_{-0.9}$	...	102.8/660 (46.1%)	1.95
J16206–5253	J161955.4–525230 (11)	$3.8^{+3.3}_{-2.6}$	$0.67^{+0.98}_{-0.90}$	$0.85^{+0.35}_{-0.19}$	...	287.7/660 (55.3%)	0.99
J16413–4046	J164119.4–404737 (12)	$6.3^{+4.1}_{-3.4}$	$0.47^{+0.76}_{-0.73}$	$2.6^{+0.7}_{-0.4}$	...	416.9/660 (81.4%)	0.41
	J164119.4–404737 (12)[f]	$3.9^{+3.9}_{-2.6}$	$0.29^{+0.94}_{-0.80}$	1.89 ± 0.47	...	8.5/9	0.41
J16560–4958	J165551.9–495732 (13)	$2.3^{+0.7}_{-0.6}$	$2.2^{+0.5}_{-0.4}$	18^{+16}_{-7}	$0.88^{+0.12}_{-0.18}$	55.9/49	0.35
J21565+5948	J215604.2+595604 (14)	$1.1^{+0.8}_{-0.6}$	1.6 ± 0.5	$1.4^{+0.6}_{-0.3}$	...	421.3/660 (77.4%)	0.65

Notes. The parameters are for power-law fits to the *Chandra*/ACIS spectra and include photoelectric absorption with cross sections from Balucinska-Church & McCammon (1992) and abundances from Wilms et al. (2000). In general, the measured value of N_H and the errors on N_H are scaled down by ~30% if solar abundances (Anders & Grevesse 1989) are used rather than the approximation to average interstellar abundances (Wilms et al. 2000). A pile-up correction was applied in the two cases where pile-up parameters are given. The PSF fraction (Davis 2001) was left fixed to 0.95 (the default value). Errors in this table are at the 90% confidence level ($\Delta C = 2.7$ for the Cash fits and $\Delta\chi^2 = 2.7$ for the χ^2 fits).

[a] Unabsorbed 0.3–10 keV flux in units of 10^{-12} erg cm^{-2} s^{-1}.

[b] The grade migration parameter in the pile-up model (Davis 2001). The probability that n events will be piled together but will still be retained after data filtering is α^{n-1}.

[c] For the Cash fits, we report the Cash statistic for the best-fit model, the degrees of freedom, and, in parentheses, the percentage of simulated spectra for which better fits were obtained. For the χ^2 fits, we report the χ^2 for the best-fit model and the degrees of freedom.

[d] The column density inferred from the Kalberla et al. (2005) H I survey.

[e] With a Gaussian emission line added with $E_{line} = 6.8^{+0.5}_{-0.4}$ keV, $\sigma_{line} = 0.45^{+0.58}_{-0.45}$ keV, and $N_{line} = (9.1^{+37}_{-6.4}) \times 10^{-5}$ photons cm^{-2} s^{-1}.

[f] With a Gaussian emission line added with $E_{line} = 5.0 \pm 0.3$ keV, $\sigma_{line} = 0.3 \pm 0.3$ keV, and $N_{line} = (1.9^{+1.7}_{-1.5}) \times 10^{-5}$ photons cm^{-2} s^{-1}.

probabilities range from 0.35% to 24%, and we would, roughly, consider the four with values between 0.35% and 1.7% to be very likely associations, the three with values between 2.2% and 3.0% to be likely associations, the seven with values between 5.1% and 8.8% to be somewhat likely associations, and the four with values of 12% or greater to be questionable. For the cases with two candidate counterparts (i.e., cases for which we know one of the counterparts is spurious), the candidates with the higher probabilities of being spurious have values of 2.2%, 12%, 18%, and 24%. Although it is somewhat surprising that one of the spurious sources has a probability of only 2.2%, the other three would fall in the "questionable" category.

The faintest sources actually become significantly more likely to be spurious when one considers that the AGN contribution causes the $\log N - \log S$ to steepen at low flux levels. Although it is clear that this steepening occurs (Hands et al. 2004; Kim et al. 2007), there are complications in the Galactic plane due to absorption of the background AGN by the ISM as well as uncertainties about the decomposition of the $\log N - \log S$ into its Galactic and extragalactic parts. However, if we take the combination of Galactic and extragalactic components estimated by Sugizaki et al. (2001), the spurious probabilities for the four faintest sources increase by factors of 1.7–2.2. The changes are much smaller for the brighter sources, but, in Table 4, we provide the spurious probabilities with the extragalactic component included for all of the *Chandra* candidates.

We also considered whether extrapolations of the *Chandra* spectra are consistent with the 20–40 keV *INTEGRAL* fluxes. To estimate the maximum extrapolated hard X-ray flux, we fixed the photon index to the lowest (i.e., hardest) value within its 90% confidence error range, refitted the spectra, and then calculated the 20–40 keV flux. The same procedure was used to determine the minimum flux, but the photon index was fixed to the highest (i.e., softest) value. Table 5 includes the 20–40 keV fluxes reported from *INTEGRAL* observations (Bird et al. 2010) along with an indication of whether each source has variable hard X-ray emission, the minimum and maximum extrapolated fluxes (with the values of the photon index used), and a conclusion about whether the measured *INTEGRAL* and extrapolated *Chandra* fluxes are consistent with one another. The fluxes are labeled either as "consistent" or "cutoff needed" in 13 cases, where the latter conclusion

Table 4
Quantities for Calculating the Probability of Spurious Associations

IGR Name	CXOU Name	$F_{2-10\,keV}$[a]	$N(>F_{2-10\,keV})$ (degrees^{-2})[b]	θ (arcmin)[c]	$\theta_{INTEGRAL}$ (arcmin)[d]	Probability (%)[e]	Probability (%)[f]
J01545+6437	J015435.2+643757 (1)	2.94×10^{-13}	3.83	1.32	4.1	5.6	8.0
J03103+5706	J031010.6+570712 (2)	2.54×10^{-13}	4.30	1.37	4.9	8.8	12.8
J09189–4418	J091858.8–441830 (3)	2.30×10^{-12}	0.77	0.64	4.5	1.4	1.5
J12489–6243	J124846.4–623743 (4a)	5.29×10^{-13}	2.37	5.42	4.1	6.1	7.9
	J124905.3–624242 (4b)	4.14×10^{-14}	13.4	1.40	4.1	24	53
J13402–6428	J133935.8–642537 (5a)	5.59×10^{-13}	2.27	5.02	3.5	5.1	6.4
	J133959.2–642444 (5b)	1.18×10^{-13}	6.82	4.29	3.5	12	21
J15293–5609	J152929.3–561213 (6)	1.30×10^{-13}	6.79	3.08	5.4	17	29
J15368–5102	J153658.6–510221 (7)	3.22×10^{-13}	3.51	1.82	4.9	7.4	10.3
J15391–5307	J153916.7–530815 (8)	8.59×10^{-13}	1.67	2.25	4.5	2.9	3.5
J15415–5029	J154126.4–502823 (9a)	5.46×10^{-13}	2.38	1.12	3.8	3.0	3.8
	J154140.5–502848 (9b)	5.11×10^{-14}	14.1	2.02	3.8	18	39
J16173–5023	J161728.2–502242 (10a)	5.87×10^{-12}	0.36	2.11	3.3	0.35	0.37
	J161720.6–502415 (10b)	5.83×10^{-13}	2.15	1.38	3.3	2.2	2.7
J16206–5253	J161955.4–525230 (11)	6.75×10^{-13}	1.68	6.09	4.6	6.4	7.9
J16413–4056	J164119.4–404737 (12)	1.74×10^{-12}	0.85	0.81	4.5	1.7	1.9
J16560–4958	J165551.9–495732 (13)	5.65×10^{-12}	0.32	0.99	4.1	0.56	0.59
J21565+5948	J215604.2+595604 (14)	8.63×10^{-13}	1.46	7.88	4.9	8.7	10.4

Notes.
[a] The absorbed 2–10 keV flux in units of erg cm^{-2} s^{-1}.
[b] The X-ray source density at the flux level for each source from the *ASCA* survey of the Galactic plane using the log N – log S from Section 3.1 (Sugizaki et al. 2001).
[c] The angular distance between the center of the *INTEGRAL* error circle and the source.
[d] The 90% confidence *INTEGRAL* error radius (Bird et al. 2010).
[e] Probability of a spurious association using the log N – log S from Section 3.1.
[f] Probability of a spurious association using a log N – log S that is the sum of the relation given in Section 3.1 and a steeper relation that is an estimate for the extragalactic contribution seen through the Galaxy (see Section 3.3).

indicates that the *Chandra* extrapolation is higher than the *INTEGRAL* flux. Three cases are labeled as "inconsistent" because the *Chandra* extrapolation is lower than the *INTEGRAL* flux. Two of these (CXOU J124905.3–624242 and CXOU J154140.5–502848) are cases with two candidate counterparts and high (18% and 24%) spurious probabilities. The third is CXOU J153658.6–510221 for which the *INTEGRAL* flux is $(3.8 \pm 0.8) \times 10^{-12}$ erg cm^{-2} s^{-1} while the maximum *Chandra* extrapolated flux is 1.8×10^{-12} erg cm^{-2} s^{-1}. Given that this is only a factor of ~2 low and that the probability for the association to be spurious is 7.4% (see Table 4), this should still be considered as a candidate counterpart.

In the final two cases (CXOU J031010.6+570712 and CXOU J152929.3–561213), no conclusion is reached because an upper limit on the 20–40 keV flux is quoted in Bird et al. (2010). This occurs because the *INTEGRAL* detection occurred in a different energy band. For CXOU J031010.6+570712, the *INTEGRAL* flux limit is $<3.8 \times 10^{-12}$ erg cm^{-2} s^{-1} while the maximum *Chandra* extrapolated flux is 2.9×10^{-12} erg cm^{-2} s^{-1}. Thus, the fluxes are formally consistent, and the association remains plausible. For CXOU J152929.3–561213, although Bird et al. (2010) report an upper limit, they also indicate that the source is variable and quote a maximum 20–40 keV flux of 2.3×10^{-12} erg cm^{-2} s^{-1}. The maximum *Chandra* extrapolated flux is 25 times lower than this, but since the source is known to be variable, we cannot rule out the association.

In summary, based on the probabilities and the flux comparisons to *INTEGRAL*, it is likely that the CXOU J124905.3–624242 and CXOU J154140.5–502848 associations are spurious. Also, due to the presence of multiple candidate counterparts, we know that one of the IGR J13402–6428 and one of the IGR J16173–5023 candidate counterparts are spurious (unless *INTEGRAL* is actually detecting unresolved flux from both of the *Chandra* sources in these cases).

3.4. Multi-wavelength Identifications

We began the search for multi-wavelength counterparts by using the SIMBAD database[11] to determine if any known source coincides with each *Chandra* source. We used the *Chandra* positions and a search radius that was large enough to include the position of the IGR source (several arcminutes in most cases as given in Table 2). We then searched for multi-wavelength counterparts to the 18 *Chandra* sources in catalogs using the VizieR database.[12] This search included all of the ~10,000 available multi-wavelength catalogs, and we used the *Chandra* positions and a search radius of 2″. This led to many identifications at optical, IR, and, in a couple cases, radio wavelengths. The search included the *Wide-field Infrared Survey Explorer*[13] (*WISE*) catalog with measurements at 3.4, 4.8, 10.2, and 23.68 μm (L, M, N, and O bands, respectively).

The Two Micron All Sky Survey (2MASS) K_s-band images are shown for the 18 *Chandra* sources in Figure 2 with

[11] See http://simbad.u-strasbg.fr/simbad.
[12] See http://webviz.u-strasbg.fr/viz-bin/VizieR.
[13] See http://irsa.ipac.caltech.edu/Missions/wise.html.

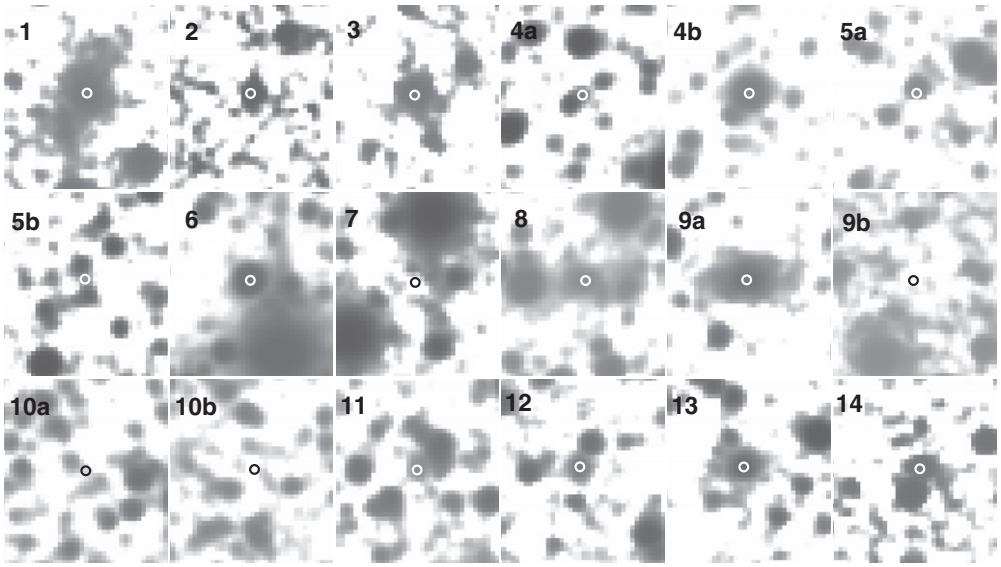

Figure 2. 2MASS K_s-band images for the 18 *Chandra* sources that are candidates for being counterparts to the IGR sources. For each image, north is up, and east is to the left. The images are approximately $40'' \times 40''$. The white and black circles mark the *Chandra* positions, and they are $1''$ in radius. The labels correspond to the sources as follows: 1, IGR J01545+6437; 2, IGR J03103+5706; 3, IGR J09189–4418; 4a, IGR J12489–6243 (candidate a); 4b, IGR J12489–6243 (candidate b); 5a, IGR J13402–6428 (candidate a); 5b, IGR J13402–6428 (candidate b); 6, IGR J15293–5609; 7, IGR J15368–5102; 8, IGR J15391–5307; 9a, IGR J15415–5029 (candidate a); 9b, IGR J15415–5029 (candidate b); 10a, IGR J16173–5023 (candidate a); 10b, IGR J16173–5023 (candidate b); 11, IGR J16206–5253; 12, IGR J16413–4046; 13, IGR J16560–4958; and 14, IGR J21565+5948.

Table 5
Comparison to *INTEGRAL* Fluxes

IGR Name	log $F_{\rm INTEGRAL}$[a]	CXOU Name	log $F_{\rm ext,min}$ (Γ)[b]	log $F_{\rm ext,max}$ (Γ)[c]	Conclusion
J01545+6437	−11.34	J015435.2+643757 (1)	−11.71 (0.16)	−10.64 (−0.99)	Consistent
J03103+5706	<−11.42	J031010.6+570712 (2)	−16.77 (7.3)	−11.54 (0.41)	...
J09189–4418	−11.64	J091858.8–441830 (3)	−11.81 (1.87)	−11.16 (1.04)	Consistent
J12489–6243	−11.42 (V)	J124846.4–623743 (4a)	−11.28 (–0.07)	−10.20 (−1.38)	Cutoff needed
		J124905.3–624242 (4b)	−17.14 (6.2)	−13.17 (1.59)	Inconsistent
J13402–6428	−11.64 (V)	J133935.8–642537 (5a)	−12.34 (1.58)	−11.36 (0.45)	Consistent
		J133959.2–642444 (5b)	−13.11 (1.53)	−10.41 (−1.13)	Consistent
J15293–5609	<−11.82 (V)	J152929.3–561213 (6)	−14.18 (2.97)	−13.04 (1.92)	...
J15368–5102	−11.42	J153658.6–510221 (7)	−12.85 (1.90)	−11.74 (0.68)	Inconsistent
J15391–5307	−11.42 (V)	J153916.7–530815 (8)	−14.56 (6.2)	−11.37 (1.11)	Consistent
J15415–5029	−11.34	J154126.4–502823 (9a)	−11.28 (0.25)	−10.52 (−0.87)	Cutoff needed
		J154140.5–502848 (9b)	−14.60 (2.83)	−12.15 (0.26)	Inconsistent
J16173–5023	−11.28	J161728.2–502242 (10a)	−11.25 (1.31)	−10.55 (0.67)	Cutoff needed
		J161720.6–502415 (10b)	−14.39 (5.4)	−9.94 (−1.38)	Consistent
J16206–5253	<−11.82	J161955.4–525230 (11)	−12.26 (1.66)	−10.78 (−0.23)	Consistent
J16413–4056	−11.52	J164119.4–404737 (12)	−11.59 (1.23)	−10.26 (−0.51)	Consistent
J16560–4958	−11.34	J165551.9–495732 (13)	−12.18 (2.69)	−11.33 (1.79)	Consistent
J21565+5948	−11.64	J215604.2+595604 (14)	−12.54 (2.11)	−11.64 (1.09)	Consistent

Notes.
[a] The base-10 logarithm of the 20–40 keV *INTEGRAL* flux reported for the source in Bird et al. (2010). Sources with evidence for 20–40 keV variability are indicated with a "V" in parentheses.
[b] Minimum 20–40 keV flux extrapolated from the *Chandra* spectrum using the value of the photon index (Γ) indicated.
[c] Maximum 20–40 keV flux extrapolated from the *Chandra* spectrum using the value of the photon index (Γ) indicated.

the *Chandra* positions marked. In 14 cases, the *Chandra* positions lie on near-IR sources and are marked with white circles. Eleven of these near-IR sources are in the 2MASS catalog. For the other three (CXOU J124846.4–623743, CXOU J133935.8–642537, and CXOU J133959.2–642444, which are labeled as 4a, 5a, and 5b in the figures and tables), the *Chandra* positions fall on blended or possibly blended near-IR sources. In four cases (CXOU J153658.6–510221, CXOU J154140.5–502848, CXOU J161728.2–502242, and CXOU J161720.6–502415, which are labeled as 7, 9b, 10a, and 10b

in the figures and tables), the *Chandra* positions, which are marked with black circles, do not fall in locations with any apparent near-IR emission.

In some cases, our multi-wavelength search confirms previously suggested counterparts, and these are discussed in Section 4.1. We obtained new multi-wavelength counterparts with the *Chandra* positions and the VizieR search described above for nine sources, and they are listed in Table 6 and discussed in Section 4.2. While the table includes the optical/IR magnitudes, we converted these to fluxes,[14] and the spectral energy distributions (SEDs) are shown in Figure 3. We fitted each SED with a blackbody with extinction to provide a rough characterization of its shape. Although none of the χ^2 values for the fits are formally acceptable, the fits show whether the SEDs are similar to a blackbody, as might be expected for a star, or if they have long-wavelength excesses, as might be expected for an AGN (Elvis et al. 1994). The spectral model accounts for interstellar extinction using the analytical approximation of Cardelli et al. (1989). The three free parameters in the fits are the blackbody temperature, the ratio of the blackbody radius to the source distance, and the number of magnitudes of extinction in the V band (A_V).

4. SPECIFIC RESULTS AND DISCUSSION FOR EACH IGR SOURCE

4.1. Confirmations of Previously Suggested Identifications

IGR J01545+6437. The position of the *Chandra* source CXOU J015435.2+643757 (1) is consistent with that of LEDA 166414, which was previously suggested as the counterpart of the IGR source (Masetti et al. 2010). Based on an optical spectrum, this source is identified as a Seyfert 2 AGN at a redshift of $z = 0.0355$ (Masetti et al. 2010). While the *Chandra* position confirms the previous identification, the spectral parameters reported in Table 3 ($N_{\rm H} = (0.0^{+0.4}_{-0.0}) \times 10^{22}$ cm^{-2}, $\Gamma = -0.40^{+0.56}_{-0.59}$) are atypical for a Seyfert 2 in that the column density is lower and the power-law index is harder than expected. We refitted the *Chandra* spectrum with the power-law index fixed to a value of $\Gamma = 1.8$, which is typical for AGNs, and we obtain $N_{\rm H} = (1.8^{+1.3}_{-0.8}) \times 10^{22}$ cm^{-2}. While these values are consistent with what is expected for a Seyfert 2 AGN, the C-statistic for this fit is 203.2 compared to 177.4 when Γ was left as a free parameter. Using `goodness` to determine the percentage of simulated spectra with a fit statistic less than that obtained for the data gives a value of 99.5%, indicating that the fit with Γ fixed is poor. We conclude that the X-ray spectrum of this source may be unusual for a Seyfert 2 AGN, but we caution that the spectrum only includes ~30 counts. It would be useful to obtain a higher quality X-ray spectrum in the future. For example, if a strong iron line is present, it could be causing the atypical value of Γ.

IGR J09189–4418. The position of the *Chandra* source CXOU J091858.8–441830 (3) is consistent with that of 2MASX J09185877–4418302, which was previously suggested as the counterpart of the IGR source based on a *Swift*/XRT position (Landi et al. 2010a). Given that it is an extended source in the near-IR, Landi et al. (2010a) suggested that the source is probably an AGN. Our measurement of $N_{\rm H} = (4.6^{+1.1}_{-1.3}) \times 10^{22}$ cm^{-2} suggests that the source may be a Seyfert 2.

[14] For cases where fluxes are not given in the catalog, we used the magnitude-to-flux converter available at http://www.gemini.edu/sciops/instruments/midir-resources/.

IGR J21565+5948. The position of the *Chandra* source CXOU J215604.2+595604 (14) is consistent with that of 2MASS J21560418+5956045, which was previously suggested as the counterpart of the IGR source based on a *Swift*/XRT position (Landi et al. 2010c). This source is also in the *ROSAT* catalog as 1RXS J215604.4+595607. Follow-up optical spectroscopy has shown that it is a Seyfert 1 AGN at a redshift of $z = 0.208$ (Bikmaev et al. 2010).

4.2. Sources of Previously Unknown Nature with Chandra Counterparts

4.2.1. IGR J03103+5706

CXOU J031010.6+570712 (2). This source is listed in the 2MASS and *WISE* catalogs. In the SED, Figure 3, the near-IR points are well described by a blackbody, but the 10 μm *WISE* point is far from the blackbody. We also obtained *R*-band images of the field of IGR J03103+5706 on the 2.4 m Hiltner telescope of the MDM Observatory on UT 2011 January 13. The Ohio-State Multi-Object Spectrograph (Martini et al. 2011) was used in imaging mode, giving a scale of 0.″273 pixel^{-1} on a University of Arizona Imaging Technology Laboratory 4064 × 4064 CCD. Five exposures of 300 s were reduced and combined using standard methods; a portion of the resulting image centered on CXOU J031010.6+570712 is shown in Figure 4. The seeing was 1.″1. A faint optical counterpart in coincidence with the X-ray candidate has position R.A. = $03^{\rm h}10^{\rm m}10.^{\rm s}55$, decl. = +57°07′12.″1 (J2000.0), measured with respect to the USNO-B1.0 catalog (Monet et al. 2003). The curve-of-growth from aperture photometry is shown in Figure 5, which clearly shows the object to be extended in comparison with the stellar PSF. The photometry was calibrated using the Landolt (1992) group of standard stars around RU 149. We measure $R = 22.30 \pm 0.11$ in a 3.″3 radius aperture, which includes all of the detectable light from this apparent galaxy. The extended nature of the source and the 10 μm excess likely indicate that the source is an AGN.

It should also be noted that CXOU J031010.6+570712 is not the same source that was previously suggested as a possible counterpart to IGR J03103+5706 by Maiorano et al. (2011). The other candidate was selected for being an extended near-IR source (2MASX J03095498+5707023) with a radio counterpart (and therefore and AGN candidate) in the *INTEGRAL* error circle. Although our `wavdetect` source detection procedure did not detect a *Chandra* source at the location of the 2MASX source, there are three ACIS counts within 3″ of the 2MASX source. Given the background rate estimate of 0.23 s^{-1} in a circular region with a 3″ radius, 3 counts corresponds to a detection at the 99.8% confidence (2.9σ) level. Even if this is a true detection, CXOU J031010.6+570712 is significantly brighter (17.4 counts), but it still raises some uncertainty about which source is the correct counterpart. This is especially true because IGR J03103+5706 was only detected by *INTEGRAL* during one satellite revolution (Bird et al. 2010), and its long-term X-ray behavior is unknown.

4.2.2. IGR J12489–6243

CXOU J124846.4–623743 (4a). Although this source is not clearly resolved from a nearby source in the 2MASS images, it becomes resolved in the GLIMPSE images. The positive slope of the two GLIMPSE points is consistent with a blackbody, but other models are certainly not ruled out. In X-rays, the source has the hardest best-fit photon index of any of our *Chandra* candidates, $\Gamma = -0.83^{+0.76}_{-0.56}$, and the upper limit on

Table 6
Optical/Infrared/Radio Identifications

Catalog	Separation[a]	Magnitudes			
IGR J03103+5706/CXOU J031010.6+570712 (2)					
2MASS	0.″47	$J = 16.82 \pm 0.15$	$H = 15.53 \pm 0.12$	$K_s = 14.72 \pm 0.10$	
WISE	0.″44	$L = 13.670 \pm 0.041$	$M = 13.261 \pm 0.042$	10.417 ± 0.246	$O > 8.348$
IGR J12489–6243/CXOU J124846.4–623743 (4a)					
GLIMPSE	0.″40	$m_{3.6} = 14.130 \pm 0.073$	$m_{4.5} = 14.031 \pm 0.107$		
IGR J12489–6243/CXOU J124905.3–624242 (4b)					
USNO-A2.0	0.″76	$B = 19.1 \pm 0.5$	$R = 15.5 \pm 0.5$		
USNO-B1.0	0.″35	$R_1 = 15.21 \pm 0.3$	$B_2 = 19.41 \pm 0.3$	$R_2 = 16.01 \pm 0.3$	$I = 13.85 \pm 0.3$
NOMAD	0.″35	$B = 17.77 \pm 0.3$	$V = 16.52 \pm 0.3$		
GSC 2.3.2	0.″08	$R = 15.42 \pm 0.43$	$V = 16.59 \pm 0.46$	$I = 13.14 \pm 0.44$	
UCAC3	0.″12	$V = 16.351 \pm 0.438$			
2MASS	0.″08	$J = 10.122 \pm 0.026$	$H = 9.090 \pm 0.022$	$K_s = 8.675 \pm 0.024$	
GLIMPSE	0.″15	$m_{3.6} = 8.256 \pm 0.035$	$m_{4.5} = 8.161 \pm 0.027$	$m_{5.8} = 8.070 \pm 0.019$	$m_{8.0} = 8.015 \pm 0.017$
DENIS	0.″31	$I = 13.26 \pm 0.02$	$J = 10.14 \pm 0.07$	$K = 8.54 \pm 0.07$	
WISE	0.″18	$L = 8.237 \pm 0.023$	$M = 8.120 \pm 0.022$	$N = 8.588 \pm 0.382$	$O > 3.628$
IGR J15293–5609/CXOU J152929.3–561213 (6)					
HST GSC	0.″14	$V = 13.00 \pm 0.28$			
USNO-B1.0	1.″32	$B_2 = 12.46 \pm 0.3$	$R_2 = 10.24 \pm 0.3$		
NOMAD	0.″25	$B = 13.13 \pm 0.3$	$V = 12.27 \pm 0.3$		
GSC 2.3.2	0.″21	$R = 11.45 \pm 0.42$	$B = 13.11 \pm 0.40$	$I = 10.32 \pm 0.36$	
UCAC3	0.″25	$V = 11.732 \pm 0.045$			
2MASS	0.″19	$J = 9.620 \pm 0.026$	$H = 8.962 \pm 0.022$	$K_s = 8.747 \pm 0.024$	
GLIMPSE	0.″20	$m_{3.6} = 8.650 \pm 0.054$	$m_{4.5} = 8.726 \pm 0.043$	$m_{5.8} = 8.571 \pm 0.037$	$m_{8.0} = 8.462 \pm 0.031$
DENIS	0.″25	$I = 10.62 \pm 0.08$	$J = 9.54 \pm 0.06$	$K = 8.71 \pm 0.06$	
DENIS	0.″26	$I = 10.70 \pm 0.05$	$J = 9.59 \pm 0.05$	$K = 8.74 \pm 0.07$	
SOGS[b]	0.″34	$V = 13.00 \pm 0.3$	$B = 13.60 \pm 0.3$		
WISE	0.″23	$L = 8.610 \pm 0.028$	$M = 8.794 \pm 0.029$	$N = 8.718 \pm 0.099$	$O > 8.059$
IGR J15391–5307/CXOU J153916.7–530815 (8)					
2MASS	0.″30	$J = 14.946$	$H = 13.946 \pm 0.081$	$K_s = 12.990 \pm 0.067$	
MGPS	0.″62	$S_{843\mathrm{MHz}} = 15.1 \pm 1.5$ mJy			
DENIS	0.″63	$J = 15.41 \pm 0.16$	$K = 13.06 \pm 0.15$		
WISE	0.″50	$L = 11.819 \pm 0.055$	$M = 11.072 \pm 0.039$	$N = 7.512 \pm 0.022$	$O = 4.829 \pm 0.025$
IGR J15415–5029/CXOU J154126.4–502823 (9a)					
USNO-A2.0	0.″49	$B = 14.9 \pm 0.5$	$R = 13.9 \pm 0.5$		
USNO-B1.0	0.″69	$R_1 = 13.88 \pm 0.3$	$B_2 = 14.73 \pm 0.3$	$R_2 = 13.29 \pm 0.3$	$I = 11.09 \pm 0.3$
NOMAD	0.″69	$B = 14.73 \pm 0.3$	$V = 16.23 \pm 0.3$		
GSC 2.3.2	0.″14	$R = 15.51 \pm 0.45$	$B = 16.46 \pm 0.51$	$V = 17.49 \pm 0.62$	$I = 12.30 \pm 0.45$
2MASS	0.″20	$J = 13.537 \pm 0.053$	$H = 12.594 \pm 0.058$	$K_s = 12.029 \pm 0.051$	
2MASX	0.″61	$J_{\mathrm{ext}} = 11.947 \pm 0.097$	$H_{\mathrm{ext}} = 11.380 \pm 0.100$	$K_{s,\mathrm{ext}} = 11.009 \pm 0.095$	
DENIS	0.″14	$I = 15.52 \pm 0.04$	$J = 13.51 \pm 0.07$	$K = 12.05 \pm 0.10$	
WISE	0.″17	$L = 11.296 \pm 0.034$	$M = 10.755 \pm 0.029$	$N = 7.229 \pm 0.020$	$O = 4.527 \pm 0.027$
IGR J16206–5253/CXOU J161955.4–525230 (11)					
2MASS	0.″21	$J = 14.701$	$H = 13.749$	$K_s = 14.183 \pm 0.124$	
GLIMPSE	0.″24	$m_{4.5} = 12.877 \pm 0.153$			
IGR J16413–4046/CXOU J164119.4–404737 (12)					
2MASS	0.″19	$J = 15.400$	$H = 15.081 \pm 0.115$	$K_s = 13.974 \pm 0.066$	
WISE	0.″24	$L = 12.599 \pm 0.107$	$M = 11.436 \pm 0.059$	$N = 8.482 \pm 0.040$	$O = 6.460 \pm 0.066$
IGR J16560–4958/CXOU J165551.9–495732 (13)					
GSC 2.3.2	0.″29	$R = 17.04 \pm 0.43$	$B = 19.24 \pm 0.41$	$I = 15.75 \pm 0.36$	
2MASS	0.″16	$J = 14.682 \pm 0.087$	$H = 13.754 \pm 0.109$	$K_s = 12.930 \pm 0.058$	
DENIS	0.″40	$I = 16.51 \pm 0.08$	$J = 14.48 \pm 0.12$	$K = 12.64 \pm 0.16$	
DENIS	0.″51	$I = 17.10 \pm 0.11$	$J = 15.04 \pm 0.13$	$K = 13.17 \pm 0.17$	
WISE	0.″20	$L = 11.507 \pm 0.035$	$M = 10.755 \pm 0.030$	$N = 8.471 \pm 0.033$	$O = 6.423 \pm 0.071$

Notes. The catalogs are the Two Micron All Sky Survey (2MASS and 2MASX; Cutri et al. 2003), the Deep Near-Infrared Survey of the Southern Sky (DENIS), the United States Naval Observatory (USNO-B1.0 and USNO-A2.0; Monet 1998; Monet et al. 2003), the Naval Observatory Merged Astrometric Dataset (NOMAD; Zacharias et al. 2005), the Guide Star Catalog (GSC 2.3.2; Lasker et al. 2008), the Third U.S. Naval Observatory CCD Astrograph Catalog (UCAC3; Zacharias et al. 2009), the Galactic Legacy Infrared Mid-Plane Survey Extraordinaire (GLIMPSE), the *Wide-field Infrared Survey Explorer* catalog (*WISE*; Cutri et al. 2011), the HST Guide Star Catalog (HST GSC; Lasker et al. 1996), the Sydney Observatory Galactic Survey (SOGS; Fresneau et al. 2007), and the Second Epoch Molonglo Galactic Plane Survey (MGPS-2; Murphy et al. 2007).

[a] The angular separation between the *Chandra* position and the catalog position.

[b] Also, it gives parallax as 0.64 ± 0.05 mas, which corresponds to a distance of 1.56 ± 0.12 kpc.

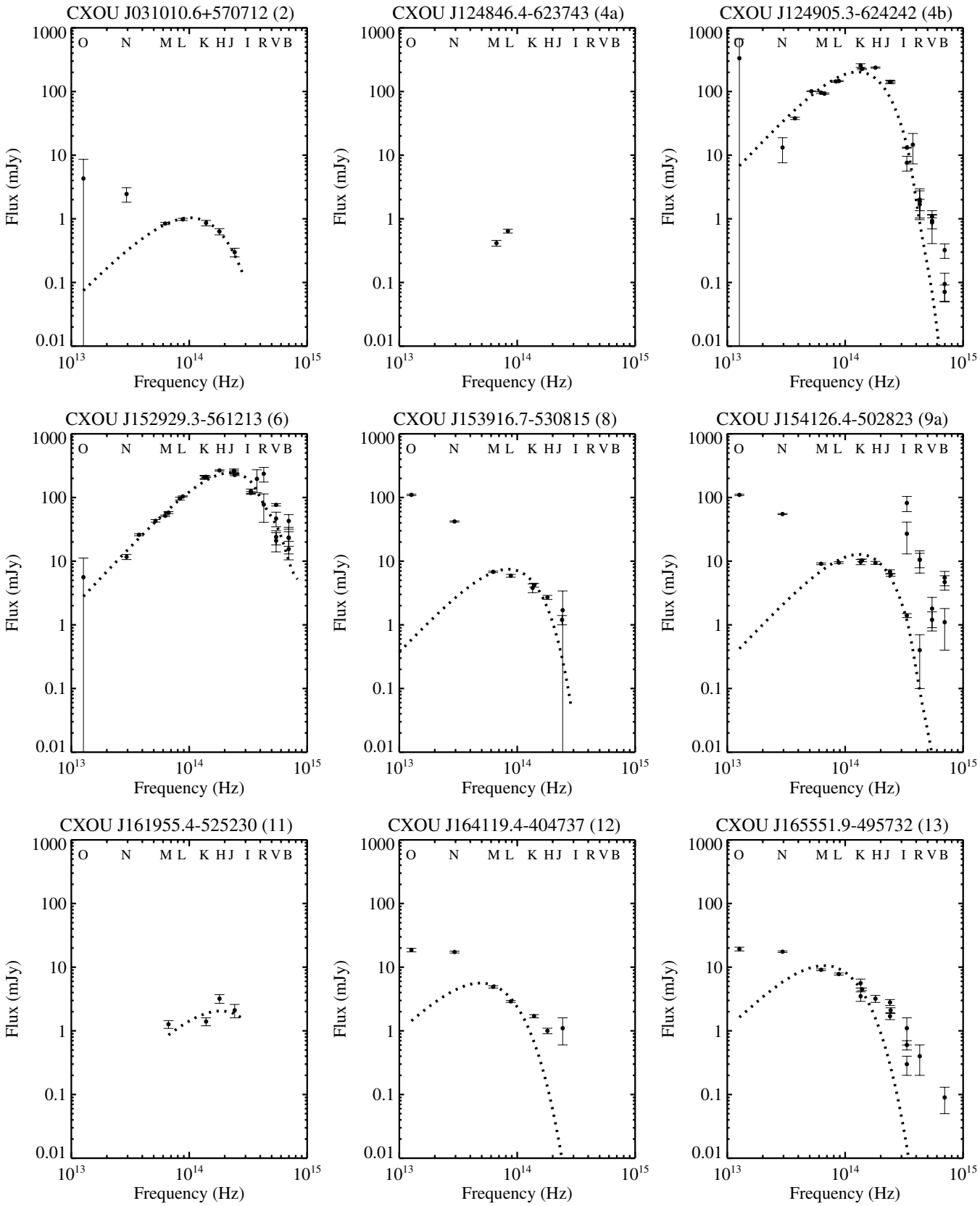

Figure 3. Optical/IR spectral energy distributions (SEDs) for the sources in Table 6. The fluxes shown are not corrected for extinction. For sources with more than three data points, the SEDs were fitted with a blackbody with extinction to determine whether they are consistent with a blackbody shape.

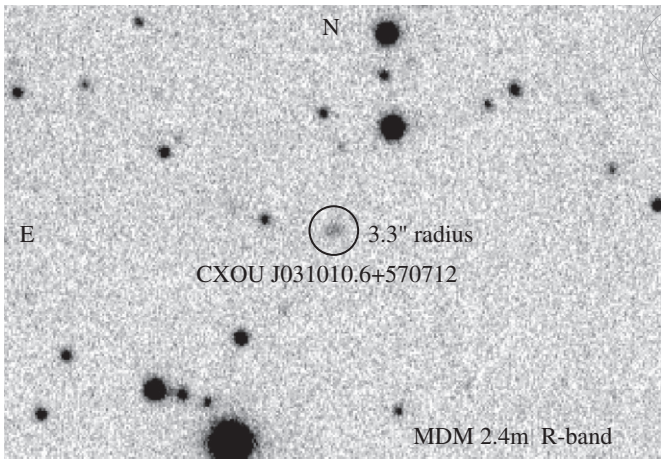

Figure 4. *R*-band image in the field of IGR J03103+5706 from the MDM Observatory 2.4 m Hiltner telescope in 1.″1 seeing. The circle of radius 3.″3 is centered on the X-ray coordinates of CXOU J031010.6+570712 (2) and was used to measure the magnitude, $R = 22.30 \pm 0.11$, for the extended (see Figure 5) optical counterpart.

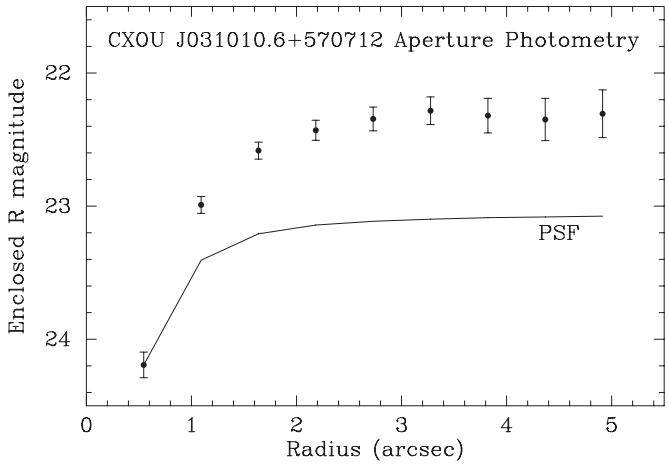

Figure 5. Aperture photometry of the extended optical counterpart of CXOU J031010.6+570712 (2) in Figure 4. The curve of growth is broader than that of a PSF star. The two curves are normalized at the smallest aperture used.

the column density ($N_{\rm H} < 1.2 \times 10^{22}$ cm^{-2}) is slightly less than the Galactic $N_{\rm H}$ along this line of sight. The properties strongly suggest a Galactic origin, but the precise nature is unclear. In addition, *INTEGRAL* detected hard X-ray variability from IGR J12489–6243 (see Table 5), which would also not be surprising for a Galactic source. The most likely possibilities for the classification are that the source is a CV or an HMXB (an LMXB is unlikely because they typically have softer X-ray spectra).

CXOU J124905.3–624242 (4b). This is a bright optical and IR source that is present in many of the catalogs. The SED shown in Figure 3 can be approximately described by a blackbody. Although there are significant deviations from a blackbody, there is no excess in the IR (e.g., below $\sim 10^{14}$ Hz in the *L* through *O* bands). It is likely that the optical/IR SED is dominated by emission from a star and that the source is Galactic. For this source, Figure 3 shows the best-fit values of $A_V \sim 13$ and $T \sim 100{,}000$ K. However, these two parameters are strongly correlated, and the temperature is as low as 3000 K for $A_V = 6$, for example. The currently available information does not allow us to rule out this level of extinction. The X-ray spectral parameters are poorly constrained, but the column density ($N_{\rm H} = (4.2^{+5.3}_{-2.9}) \times 10^{22}$ cm^{-2}) either suggests that the source is at a relatively large distance or that it has some level of intrinsic absorption. However, it is important to keep in mind that the softness of the power-law component makes this source less likely than candidate 4a to be the counterpart to the IGR source.

4.2.3. IGR J13402–6428

CXOU J133935.8–642537 (5a). The *Chandra* position for this source falls 1.″4 from 2MASS J13393589–6425363, which is a large enough difference to make the *Chandra*/2MASS association unlikely. The K_s-band magnitude for the 2MASS source is 12.53 ± 0.03, and a better near-IR image is needed to constrain the level of near-IR emission from the *Chandra* source.

CXOU J133959.2–642444 (5b). This *Chandra* source falls between two $K_s \sim 14$ stars. The *Chandra* position is >3″ from both of these stars, ruling out an association with either of them, and a better near-IR image is needed to determine if there is a fainter near-IR source between the two stars.

4.2.4. IGR J15293–5609

CXOU J152929.3–561213 (6). This is a bright optical and IR source that appears to be point-like. Its SED is well constrained from the *N*-band to the optical and is well described by a blackbody with no evidence for an IR excess. The source appears in the Sydney Observatory Galactic Survey (SOGS) catalog (Fresneau et al. 2007), and this survey includes a parallax measurement for the source, indicating that it is at a distance of 1.56 ± 0.12 kpc. The fact that the X-ray column density is $N_{\rm H} = (3.4^{+2.8}_{-2.3}) \times 10^{21}$ cm^{-2}, which is significantly below the Galactic column density along this line of sight (1.56×10^{22} cm^{-2}), is consistent with a relatively nearby source. The 0.3–10 keV X-ray luminosity is $(1.4^{+1.0}_{-0.4}) \times 10^{32}$ erg s^{-1}.

In this case, it is possible to use the blackbody fit to the SED to constrain the spectral type of the star. From the measured $N_{\rm H}$ value, we derive $A_V = 1.5^{+1.3}_{-1.0}$ using the relationship given in Güver & Özel (2009). At values of A_V corresponding to the minimum (0.5), the best estimate (1.5), and the maximum (2.7), the blackbody temperatures are 4200, 5100, and 7000 K, respectively. At a distance of 1.56 kpc, the blackbody radii for these three temperatures are 16.4, 14.5, and 12.0 $R_\odot$. The temperatures are consistent with the star being a K-type or a G-type giant, but the radii are more consistent with an early K-type giant (Cox 2000). Thus, we suggest that IGR J15293–5609 is a symbiotic system with a luminosity class III donor. Given the X-ray luminosity quoted above, the accretor is most likely to be a white dwarf.

4.2.5. IGR J15368–5102

CXOU J153658.6–510221 (7). No counterparts are present in any of the multi-wavelength catalogs at the *Chandra* position of this source. In addition, it is clear from the K_s-band image (Figure 2) that any near-IR counterpart must be below the 2MASS detection threshold.

4.2.6. IGR J15391–5307

CXOU J153916.7–530815 (8). We previously reported on the *Chandra* position and the 2MASS association for this source (Tomsick et al. 2011b). Based on the 2MASS magnitudes and

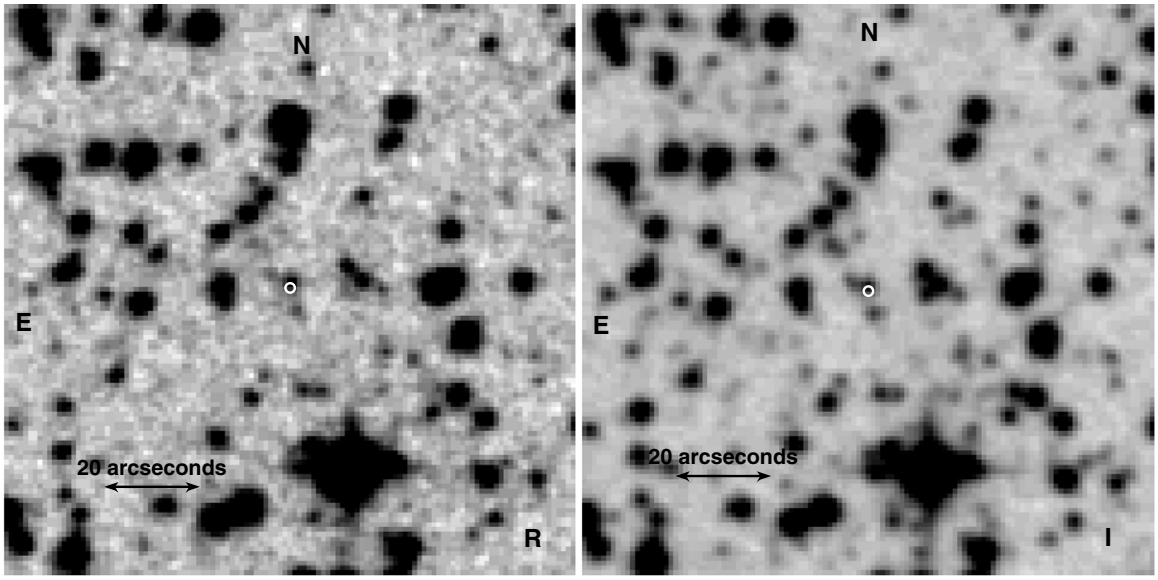

Figure 6. *R*- and *I*-band images for the field around CXOU J161728.2–502242 (10a). The white circle marks the position of the *Chandra* source and has a radius of 1″. The nearby optical source is 0.″67 away in the USNO-A2.0 catalog and 0.″93 away in the USNO-B1.0 catalog, which is marginally consistent with the *Chandra* position. The *R* and *I* magnitudes are both near 17.

the very high $N_{\rm H}$ from the X-ray spectrum, we concluded that the source probably has intrinsic absorption, which is possible either for an HMXB or an AGN (Seyfert 2). The new information we have obtained in this work is that the source is also a 15.1 ± 1.5 mJy radio source (see Table 6) as well as having a strong IR component with fluxes in *N* and *O* bands that are orders of magnitude above the blackbody fit (see Figure 3). This strongly favors the AGN hypothesis, and this source is very likely a Seyfert 2 galaxy.

4.2.7. IGR J15415–5029

CXOU J154126.4–502823 (9a). This source is in the 2MASS catalog of extended sources (2MASX J15412638–5028233), and the fact that it is extended is clear from Figure 2. It has also been identified with the galaxy LEDA 3077397/WKK98 5204 (Woudt & Kraan-Korteweg 2001). The SED in Figure 3 shows a strong IR excess with a rising flux all the way to the longest *WISE* wavelength (*O* band). In addition, this source is likely associated with the 77.3 ± 2.9 mJy radio source, MGPS J154126–502823 (Murphy et al. 2007). Although the radio source is 2.″2 from the *Chandra* position, the rms (68% confidence) uncertainty on the radio position is 1.″7 and 1.″9 in R.A. and decl., respectively. Thus, the *Chandra* and radio positions are consistent within errors that are only slightly larger than the 1σ level. This information all points to the source being an AGN, and it may be a Seyfert 1 since the column density is relatively low $N_{\rm H} < 1.1 \times 10^{22}$ cm^{-2}. The large amount of scatter in the optical part of the SED may indicate variability. We note that this source fits in well with the Maiorano et al. (2011) efforts to identify AGN among IGR sources using the 2MASX and radio catalogs.

CXOU J154140.5–502848 (9b). No counterparts are present in any of the multi-wavelength catalogs at the *Chandra* position of this source. In addition, it is clear from the K_s-band image (Figure 2) that any near-IR counterpart must be below the 2MASS detection threshold. Based on the X-ray information for this source (9b) and 9a, we argue that 9a is a much more likely candidate, and the fact that 9a is an AGN makes it even more strongly favored as being identified with IGR J15415–5029.

4.2.8. IGR J16173–5023

CXOU J161728.2–502242 (10a). In this case, the catalog search was somewhat ambiguous. The closest 2MASS source is 4.″2 away from the *Chandra* position, and the sources are clearly not associated (see also Figure 2). However, the search uncovered an optical source in the USNO catalogs that is only 0.″67 away (in USNO-A2.0) and 0.″93 away (in USNO-B1.0) from the *Chandra* position, and these might be associated. Figure 6 shows *R*- and *I*-band images from the Digitized Sky Survey, and although the images are not of sufficient quality to be certain, the association appears to be plausible. In USNO-B1.0, the optical magnitudes of this source are $B_2 = 18.15$, $R_1 = 17.02$, $R_2 = 17.08$, and $I = 17.14$. In addition, the SIMBAD search showed that the *Chandra* position is consistent with that of the soft X-ray (0.1–2.4 keV) *ROSAT* source 1RXS J161728.1–502238. The photon index measured by *Chandra* for this source is relatively hard $\Gamma = 0.97^{+0.34}_{-0.30}$, but the *ROSAT* detection and the column density of $N_{\rm H} = (5.7^{+3.1}_{-2.5}) \times 10^{21}$ cm^{-2}, which is significantly less than the Galactic column density of 1.94×10^{22} cm^{-2}, indicate that the source is Galactic and that it may be relatively nearby. The optical counterpart, if it is truly associated with the source, as well as the possible iron line seen in the *Chandra* spectrum (see Table 3) are also consistent with the source being in the Galaxy. Due to the lack of a near-IR counterpart, the source is not an HMXB, but its hard X-ray power law and its possible optical counterpart may suggest that it is a magnetic CV.

CXOU J161720.6–502415 (10b). While the closest 2MASS source to this *Chandra* position is 7.″3 away, the catalog search uncovered a closer source in the GLIMPSE catalog. This IR source is 0.″87 from the *Chandra* position, which is only marginally consistent given the 90% confidence *Chandra* position uncertainty of 0.″64. Also, we note that for the *Chandra* sources that do have GLIMPSE counterparts given in Table 6, the separations are between 0.″15 and 0.″40. While we doubt this association, the *Chandra* spectrum allows for a very high column density, $N_{\rm H} = (2.2^{+3.9}_{-1.9}) \times 10^{23}$ cm^{-2}, which could suggest that the source is an obscured HMXB or a

Seyfert 2 AGN. For both source types, an IR counterpart would be expected. However, due to the uncertainty on the $N_{\rm H}$ measurement and the marginal IR counterpart association, we are not able to narrow down the possibilities for this source.

4.2.9. IGR J16206–5253

CXOU J161955.4–525230 (11). This source appears in the 2MASS and GLIMPSE catalogs. Although the 2MASS image (see Figure 2) shows that it is blended with other sources, there is no evidence that it is extended. There are only four points in the SED (see Figure 3), but it shows that the near-IR fluxes are consistent with a blackbody (but other models are certainly not ruled out). The source is not in the *WISE* catalog, so there is no evidence for an IR excess that could be the signature of an AGN. Thus, we suspect that the source is Galactic, but the X-ray and multi-wavelength information do not provide any further hints to the nature of this source.

4.2.10. IGR J16413–4046

CXOU J164119.4–404737 (12). Previously, *Swift*/XRT observed the IGR J16413–4046 field, and the presence of a soft X-ray counterpart was reported (Landi et al. 2010b, 2011). The position of the *Chandra* source is consistent with the *Swift* source, and the refined *Chandra* position has provided a 2MASS identification (see Tomsick et al. 2011a, and Table 6). The absorbed 2–10 keV flux measured by *Swift* in 2011 January is 1.4×10^{-12} erg cm^{-2} s^{-1}, and our 2011 May *Chandra* measurement is $(1.7 \pm 0.5) \times 10^{-12}$ erg cm^{-2} s^{-1}, which is consistent with no soft X-ray variability between these two observations. The SED (Figure 3) is not well described by a blackbody. There is a strong IR excess based on the *WISE* fluxes, and it appears that the SED has approximately a broken power-law shape (although it should be noted that the SED is not corrected for extinction). The SED suggests a non-thermal origin to the emission, which could indicate a jet from an AGN or an X-ray binary. The lack of variability may suggest that an AGN is more likely. Also, if the marginally detected 5 keV emission line is real, then this would make the AGN possibility certain. For X-ray spectral fits with and without the emission line, the column density significantly exceeds the Galactic value of $N_{\rm H} = 4.1 \times 10^{21}$ cm^{-2}. Thus, if the source is an AGN, it is likely a Seyfert 2.

4.2.11. IGR J16560–4958

CXOU J165551.9–495732 (13). The SED for this source is very similar to CXOU J164119.4–404737 with an IR excess and a broken power-law shape. Although a detailed modeling of the SED is beyond the scope of this paper, the apparent curvature in the optical part of the SED (see Figure 3) may be due to extinction. This source has the highest *Chandra* count rate of any source in our study, and we obtained a relatively good constraint on the column density, $N_{\rm H} = (2.3^{+0.7}_{-0.6}) \times 10^{22}$ cm^{-2}, which is significantly above the Galactic value of $N_{\rm H} = 3.5 \times 10^{21}$ cm^{-2}. This source may be a Seyfert 2 AGN, but it was recently selected as a blazar candidate based on its IR colors in the *WISE* catalog (Massaro et al. 2012). Although Massaro et al. (2012) did not have a soft X-ray position for IGR J16560–4958, we confirm that the *WISE* counterpart they identified is the same one that we identified in Table 6.

4.3. IGR Sources without Likely Candidate Counterparts

For four of the IGR sources, the *Chandra* observations do not result in any candidate counterparts that stand out from the general X-ray source population. One of these sources, IGR J21188+4901, was found to be highly variable from the *INTEGRAL* observations (Bird et al. 2010). The source was classified as one of the sources having variability by more than a factor of four, and Bird et al. (2010) report a peak 20–40 keV flux of 4.5 ± 1.3 mCrab and an average 20–40 keV flux of <0.2 mCrab, indicating a difference by a factor of >16. Thus, this source appears to be a transient. In addition, IGR J04069+5042 and IGR J06552–1146 are classified in Bird et al. (2010) as being variable by factors of between 1.1 and 4. While these relatively small factors do not prove that these sources are transients, the variability is likely the reason that no bright source was detected by *Chandra*. IGR J22014+6034 is not indicated as being variable in Bird et al. (2010). If soft X-ray counterparts are identified in the future (e.g., during outbursts from the variable or transient sources), then the tables of detected sources given in the Appendix will be useful for understanding their long-term X-ray behavior.

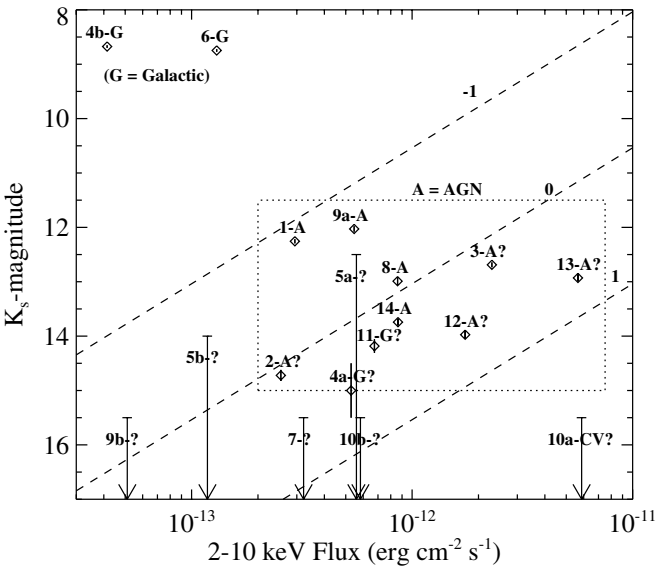

Figure 7. Summary plot showing the absorbed 2–10 keV fluxes vs. the K_s-band magnitudes for the *Chandra* sources. The source types are A = AGN, G = Galactic, CV = cataclysmic variable, and ? = unknown. A question mark after one of the source types indicates some uncertainty about that identification. The dotted box shows the region where the eight AGNs or likely AGNs lie. The dashed lines mark constant values of $\log(f_X/f_{K_s})$ equal to –1, 0, and 1, and allow for comparison to the AGNs studied by Watanabe et al. (2004). The labels correspond to the sources as follows: 1, IGR J01545+6437; 2, IGR J03103+5706; 3, IGR J09189–4418; 4a, IGR J12489–6243 (candidate a); 4b, IGR J12489–6243 (candidate b); 5a, IGR J13402–6428 (candidate a); 5b, IGR J13402–6428 (candidate b); 6, IGR J15293–5609; 7, IGR J15368–5102; 8, IGR J15391–5307; 9a, IGR J15415–5029 (candidate a); 9b, IGR J15415–5029 (candidate b); 10a, IGR J16173–5023 (candidate a); 10b, IGR J16173–5023 (candidate b); 11, IGR J16206–5253; 12, IGR J16413–4046; 13, IGR J16560–4958; and 14, IGR J21565+5948.

5. SUMMARY AND CONCLUSIONS

While we expect follow-up observations, especially optical and near-IR spectroscopy, to provide definite identifications of the nature of many of these sources, the *Chandra* observations have allowed us to determine the nature of some of the IGR sources as well as providing *Chandra* counterpart identifications for 14 of the 18 sources. A summary is provided in Table 7, indicating that four of the IGR sources show definite or very strong evidence for being AGNs. IGR J01545+6437 and IGR J21565+5948 both have redshift measurements,

Table 7
Summary of Results for the IGR Sources

IGR Name	Remaining *Chandra* Candidate Counterparts	Source Type	Evidence
J01545+6437	CXOU J015435.2+643757 (1)	AGN	LEDA 166414, $z = 0.0355$
J03103+5706	CXOU J031010.6+570712 (2)	AGN?	IR excess, optical extension
J04069+5042	...	...	...
J06552–1146	...	...	...
J09189–4418	CXOU J091858.8–441830 (3)	AGN?	2MASX J09185877–4418302
J12489–6243	CXOU J124846.4–623743 (4a) CXOU J124905.3–624242 (4b)	Galactic? Galactic	SED slope, hard X-ray spectrum Blackbody SED
J13402–6428	CXOU J133935.8–642537 (5a) CXOU J133959.2–642444 (5b)	? ?	... ...
J15293–5609	CXOU J152929.3–561213 (6)	Galactic[a]	Parallax, blackbody SED
J15368–5102	CXOU J153658.6–510221 (7)	?	...
J15391–5307	CXOU J153916.7–530815 (8)	AGN	Radio emission, IR excess
J15415–5029	CXOU J154126.4–502823 (9a)	AGN	2MASX J15412638–5028233, WKK98 5204
J16173–5023	CXOU J161728.2–502242 (10a) CXOU J161720.6–502415 (10b)	CV? ?	Low $N_{\rm H}$, optical counterpart? ...
J16206–5253	CXOU J161955.4–525230 (11)	Galactic?	SED slope
J16413–4046	CXOU J164119.4–404737 (12)	AGN?	IR excess, 5 keV Fe line?
J16560–4958	CXOU J165551.9–495732 (13)	AGN?	IR excess
J21188+4901	...	Transient	...
J21565+5948	CXOU J215604.2+595604 (14)	AGN	$z = 0.208$
J22014+6034	...	...	...

Notes.
[a] Based on the optical/IR spectral energy distribution and the X-ray luminosity, we suggest that this source is a symbiotic binary with an early K-type giant donor and a white dwarf accretor.

IGR J15391–5307 has a strong IR excess and radio emission, and IGR J15415–5029 is identified with the Galaxy WKK98 5204 (2MASX J15412638–5028233). IGR J15415–5029 is one of the IGR sources for which we considered two *Chandra* candidate counterparts (9a and 9b), but we strongly suspect that 9a is the correct counterpart. Four other sources (IGR J03103+5706, IGR J09189–4418, IGR J16413–4046, and IGR J16560–4958) are likely AGNs, and we label them as "AGN?" in Table 7. For these sources, the evidence is extended optical or IR emission or an IR excess (or both features).

The remaining six IGR sources for which we obtained one or two possible *Chandra* identifications may be Galactic sources. If the identification of IGR J15293–5609 with CXOU J152929.3–561213 is correct, then this is a definite Galactic source based on a parallax measurement that puts it distance at 1.56 ± 0.12 kpc. Furthermore, based on the temperature and radius inferred from a blackbody fit to its optical/IR SED, it is likely a symbiotic binary with an early K-type giant donor, and its X-ray luminosity suggests a white dwarf accretor. IGR J16206–5253 has *Chandra* and near-IR counterparts, and we argue from its SED that it is likely Galactic. IGR J12489–6243 and IGR J16173–5023 may be Galactic; however, there are still two possible *Chandra* counterparts for each source, and, in each case, there is some uncertainty about the nature of at least one of the counterparts. Once the nature of each of the *Chandra* counterparts is determined via follow-up measurements, it should become clear which counterpart is the most likely to be able to produce the hard X-ray emission detected with *INTEGRAL*. IGR J15368–5102 has a *Chandra* counterpart, and IGR J13402–6428 has two possible *Chandra* counterparts. However, the natures of these sources are still unclear.

Figure 7 shows a plot of the K_s-magnitudes and the absorbed 2–10 keV X-ray fluxes for the *Chandra* counterparts. The eight AGNs or likely AGNs fall within a range of K_s-magnitudes between 14.7 and 12.0 and within a range of X-ray fluxes between 2.5×10^{-13} and 5.7×10^{-12} erg cm^{-2} s^{-1}. We compare these ranges to a previous study of AGNs selected by 2–10 keV fluxes measured by *ASCA*. Watanabe et al. (2004) show a similar K_s versus 2–10 keV X-ray flux for ~100 *ASCA*-detected AGNs, and plot lines of constant $\log(f_X/f_{K_s})$. They find that the *ASCA* AGNs mostly fall between values of $\log(f_X/f_{K_s})$ 0 and 1, and Figure 7 shows that five of our AGNs or likely AGNs (2, 3, 12, 13, and 14) fall in that range. Watanabe et al. (2004) also included a sample of *Chandra* AGNs in their study, and a significant fraction of those AGNs have $\log(f_X/f_{K_s})$ values ranging from –1 to 0. Three of our AGNs (1, 8, 9a) fall in this range. Thus, we conclude that the near-IR and X-ray fluxes that we find for our AGNs are fairly typical.

Galactic sources are not expected to be well localized in a near-IR/X-ray flux plot, and Figure 7 shows that our Galactic or potentially Galactic sources are spread throughout the plot. The two sources with well-measured blackbody spectra are in the near-IR-bright/X-ray-faint corner of the diagram. The rest of these are relatively faint in the near-IR but have a wide range of

Table 8
Chandra Candidate Counterparts to IGR J04069+5042

Source Number	θ[a] (arcminutes)	*Chandra* R.A. (J2000)	*Chandra* Decl. (J2000)	ACIS Counts[b]	Position Uncertainty[c]	Hardness[d]
1	0.28	$04^h06^m54^s.30$	$+50°41'53''.0$	5.4	$0''.53$	-0.07 ± 0.78
2	2.80	$04^h06^m48^s.69$	$+50°39'31''.2$	3.4	$1''.17$	...
3	3.19	$04^h06^m43^s.99$	$+50°44'46''.2$	5.4	$1''.02$	-1.19 ± 1.10
4	4.70	$04^h06^m25^s.94$	$+50°41'21''.1$	5.5	$1''.78$	-0.64 ± 0.95
5	5.76	$04^h07^m17^s.11$	$+50°46'42''.9$	3.5	$3''.97$	...
6	5.82	$04^h06^m58^s.87$	$+50°47'54''.8$	3.5	$4''.07$	...
7	6.35	$04^h06^m15^s.91$	$+50°40'49''.8$	3.5	$5''.08$	...
8	6.45	$04^h07^m07^s.51$	$+50°48'16''.1$	6.5	$3''.08$	$+0.54 \pm 0.80$
9	6.85	$04^h07^m34^s.23$	$+50°45'04''.5$	13.3	$2''.03$	$+0.73 \pm 0.53$
10	7.63	$04^h06^m45^s.95$	$+50°34'37''.7$	4.3	$6''.97$	...
11	8.58	$04^h06^m48^s.17$	$+50°50'37''.5$	10.3	$4''.33$	-0.13 ± 0.55
12	9.16	$04^h05^m59^s.00$	$+50°44'17''.3$	3.3	$15''.80$	...
13	9.54	$04^h07^m38^s.06$	$+50°35'25''.6$	24.3	$2''.89$	-1.21 ± 0.43

Notes.
[a] The angular distance between the center of the *INTEGRAL* error circle, which is also the approximate *Chandra* aimpoint, and the source.
[b] The number of ACIS-I counts detected (after background subtraction) in the 0.3–10 keV band.
[c] The 95% confidence statistical uncertainty on the position using Equation (5) from Hong et al. (2005). This does not include the systematic pointing error, which is $0''.64$ at 90% confidence and $1''$ at 99% confidence.
[d] The hardness is given by $(C_2 - C_1)/(C_2 + C_1)$, where C_2 is the number of counts in the 2–10 keV band and C_1 is the number of counts in the 0.3–2 keV band.

Table 9
Chandra Candidate Counterparts to IGR J06552–1146

Source Number	θ[a] (arcminutes)	*Chandra* R.A. (J2000)	*Chandra* Decl. (J2000)	ACIS Counts[b]	Position Uncertainty[c]	Hardness[d]
1	2.99	$06^h55^m11^s.78$	$-11°49'09''.6$	2.4	$1''.61$	...
2	3.03	$06^h54^m58^s.66$	$-11°45'02''.0$	3.4	$1''.28$	...
3	3.33	$06^h55^m23^s.65$	$-11°46'01''.1$	13.4	$0''.68$	-0.62 ± 0.46
4	3.34	$06^h55^m20^s.25$	$-11°48'25''.3$	5.4	$1''.07$	$+0.68 \pm 0.89$
5	3.43	$06^h54^m56^s.31$	$-11°45'34''.6$	2.4	$1''.93$	...
6	3.65	$06^h55^m04^s.35$	$-11°42'49''.5$	5.4	$1''.20$	$+0.31 \pm 0.80$
7	3.67	$06^h55^m24^s.51$	$-11°45'11''.9$	3.4	$1''.66$	...
8	3.96	$06^h55^m05^s.48$	$-11°42'24''.2$	2.4	$2''.44$	...
9	4.10	$06^h54^m57^s.70$	$-11°43'26''.2$	2.5	$2''.52$	...
10	4.15	$06^h54^m58^s.31$	$-11°49'11''.3$	8.5	$1''.09$	-0.75 ± 0.70
11	4.43	$06^h55^m02^s.70$	$-11°50'14''.6$	7.5	$1''.30$	$+0.35 \pm 0.67$
12	4.63	$06^h55^m05^s.95$	$-11°41'40''.8$	8.5	$1''.29$	$+0.90 \pm 0.74$
13	5.03	$06^h55^m24^s.96$	$-11°49'40''.2$	9.5	$1''.38$	-0.14 ± 0.54
14	5.46	$06^h55^m04^s.96$	$-11°51'30''.6$	10.5	$1''.50$	$+0.92 \pm 0.64$
15	5.46	$06^h54^m55^s.96$	$-11°50'25''.7$	7.5	$1''.90$	$+0.35 \pm 0.67$
16	5.53	$06^h55^m29^s.56$	$-11°49'00''.1$	35.5	$0''.81$	$+0.02 \pm 0.22$
17	5.80	$06^h55^m32^s.52$	$-11°44'20''.7$	2.5	$5''.40$	...
18	5.89	$06^h55^m23^s.26$	$-11°41'16''.4$	2.5	$5''.61$	...
19	6.17	$06^h55^m34^s.57$	$-11°44'44''.0$	4.5	$3''.78$	...
20	6.22	$06^h55^m32^s.00$	$-11°43'03''.7$	16.5	$1''.44$	-0.14 ± 0.36
21	6.22	$06^h54^m48^s.69$	$-11°49'33''.7$	8.5	$2''.28$	-0.75 ± 0.70
22	6.28	$06^h54^m49^s.20$	$-11°42'33''.4$	4.5	$3''.95$	...
23	6.43	$06^h55^m24^s.04$	$-11°40'45''.5$	7.5	$2''.71$	-0.98 ± 0.84
24	6.57	$06^h55^m15^s.12$	$-11°39'44''.9$	15.5	$1''.67$	-0.73 ± 0.45
25	8.46	$06^h55^m29^s.25$	$-11°53'14''.3$	7.4	$5''.62$	-0.82 ± 0.88

Notes.
[a] The angular distance between the center of the *INTEGRAL* error circle, which is also the approximate *Chandra* aimpoint, and the source.
[b] The number of ACIS-I counts detected (after background subtraction) in the 0.3–10 keV band.
[c] The 95% confidence statistical uncertainty on the position using Equation (5) from Hong et al. (2005). This does not include the systematic pointing error, which is $0''.64$ at 90% confidence and $1''$ at 99% confidence.
[d] The hardness is given by $(C_2 - C_1)/(C_2 + C_1)$, where C_2 is the number of counts in the 2–10 keV band and C_1 is the number of counts in the 0.3–2 keV band.

Table 10
Chandra Candidate Counterparts to IGR J21188+4901

Source Number	θ[a] (arcminutes)	*Chandra* R.A. (J2000)	*Chandra* Decl. (J2000)	ACIS Counts[b]	Position Uncertainty[c]	Hardness[d]
1	3.26	$21^h18^m39^s.09$	+48°58′05″.5	4.3	1″.20	...
2	4.31	$21^h18^m47^s.81$	+49°05′19″.6	5.3	1″.57	-0.83 ± 0.97
3	4.53	$21^h18^m20^s.23$	+49°00′43″.0	4.1	2″.07	...
4	4.83	$21^h18^m54^s.59$	+48°56′19″.2	6.1	1″.74	$+0.56 \pm 0.85$
5	5.64	$21^h19^m22^s.04$	+49°00′34″.2	3.1	4″.18	...
6	5.91	$21^h18^m14^s.22$	+49°03′11″.8	3.1	4″.70	...
7	6.46	$21^h18^m52^s.15$	+49°07′26″.3	7.1	2″.87	$+0.62 \pm 0.77$
8	6.79	$21^h18^m22^s.86$	+49°06′26″.7	7.1	3″.24	-0.78 ± 0.82
9	6.87	$21^h18^m39^s.76$	+48°54′16″.7	5.5	4″.16	-1.38 ± 1.48
10	7.05	$21^h19^m17^s.20$	+48°55′53″.1	3.5	6″.75	...
11	7.29	$21^h18^m29^s.41$	+48°54′22″.7	2.5	10″.15	...
12	7.95	$21^h18^m13^s.45$	+48°55′24″.5	10.5	3″.48	$+0.14 \pm 0.55$
13	8.04	$21^h18^m03^s.40$	+49°04′26″.9	6.5	5″.48	$+1.46 \pm 1.32$
14	8.62	$21^h19^m40^s.33$	+49°01′17″.6	8.5	5″.21	$+0.88 \pm 0.82$
15	8.96	$21^h18^m24^s.93$	+48°52′53″.2	5.5	8″.85	$+0.82 \pm 1.15$
16	8.97	$21^h18^m58^s.24$	+49°09′49″.3	6.5	7″.54	$+0.23 \pm 0.82$
17	9.74	$21^h19^m29^s.26$	+49°07′59″.9	3.5	18″.20	...

Notes.
[a] The angular distance between the center of the *INTEGRAL* error circle, which is also the approximate *Chandra* aimpoint, and the source.
[b] The number of ACIS-I counts detected (after background subtraction) in the 0.3–10 keV band.
[c] The 95% confidence statistical uncertainty on the position using Equation (5) from Hong et al. (2005). This does not include the systematic pointing error, which is 0″.64 at 90% confidence and 1″ at 99% confidence.
[d] The hardness is given by $(C_2 - C_1)/(C_2 + C_1)$, where C_2 is the number of counts in the 2–10 keV band and C_1 is the number of counts in the 0.3–2 keV band.

Table 11
Chandra Candidate Counterparts to IGR J22014+6034

Source Number	θ[a] (arcminutes)	*Chandra* R.A. (J2000)	*Chandra* Decl. (J2000)	ACIS Counts[b]	Position Uncertainty[c]	Hardness[d]
1	0.97	$22^h01^m25^s.01$	+60°34′03″.0	4.4	0″.62	...
2	1.26	$22^h01^m36^s.82$	+60°33′50″.2	3.4	0″.74	...
3	1.79	$22^h01^m15^s.12$	+60°32′55″.2	8.4	0″.56	$+0.56 \pm 0.61$
4	2.13	$22^h01^m09^s.34$	+60°34′08″.7	14.4	0″.50	-0.79 ± 0.46
5	2.41	$22^h01^m46^s.26$	+60°33′56″.9	5.4	0″.78	-0.43 ± 0.82
6	3.27	$22^h01^m13^s.28$	+60°31′11″.5	4.4	1″.19	...
7	3.27	$22^h01^m26^s.91$	+60°30′44″.7	3.4	1″.41	...
8	3.44	$22^h01^m06^s.43$	+60°31′38″.8	3.4	1″.51	...
9	3.51	$22^h01^m16^s.68$	+60°37′18″.6	8.4	0″.89	$+0.79 \pm 0.67$
10	3.87	$22^h01^m57^s.40$	+60°33′11″.5	6.4	1″.17	$+0.73 \pm 0.79$
11	4.49	$22^h01^m30^s.94$	+60°29′33″.6	2.7	2″.82	...
12	4.61	$22^h01^m15^s.05$	+60°38′24″.1	4.7	1″.93	...
13	4.67	$22^h01^m18^s.31$	+60°38′34″.5	2.7	3″.06	...
14	5.34	$22^h01^m54^s.13$	+60°38′09″.5	31.7	0″.81	-0.61 ± 0.27
15	5.89	$22^h02^m13^s.69$	+60°32′54″.4	4.7	3″.25	...
16	6.11	$22^h02^m08^s.35$	+60°30′42″.4	10.7	1″.85	-1.15 ± 0.70
17	6.12	$22^h01^m21^s.87$	+60°40′06″.9	28.7	1″.04	$+0.13 \pm 0.25$
18	6.13	$22^h02^m15^s.84$	+60°35′01″.3	4.7	3″.58	...
19	6.19	$22^h01^m30^s.48$	+60°40′11″.3	4.7	3″.67	...
20	6.32	$22^h01^m41^s.45$	+60°40′04″.2	2.7	6″.32	...
21	6.94	$22^h00^m31^s.63$	+60°32′27″.1	3.8	5″.99	...
22	7.29	$22^h00^m58^s.94$	+60°27′34″.7	16.8	1″.98	$+0.19 \pm 0.38$
23	7.87	$22^h02^m08^s.45$	+60°28′04″.0	2.8	11″.50	...
24	8.05	$22^h00^m21^s.14$	+60°33′41″.8	45.8	1″.35	-0.91 ± 0.25
25	8.90	$22^h02^m03^s.44$	+60°26′21″.8	3.8	12″.53	...
26	9.55	$22^h01^m43^s.90$	+60°24′42″.7	8.8	6″.80	-1.24 ± 0.91
27	10.02	$22^h01^m40^s.46$	+60°24′09″.0	18.8	4″.00	$+0.17 \pm 0.35$
28	10.38	$22^h02^m03^s.26$	+60°24′40″.3	3.8	20″.66	...

Notes.
[a] The angular distance between the center of the *INTEGRAL* error circle, which is also the approximate *Chandra* aimpoint, and the source.
[b] The number of ACIS-I counts detected (after background subtraction) in the 0.3–10 keV band.
[c] The 95% confidence statistical uncertainty on the position using Equation (5) from Hong et al. (2005). This does not include the systematic pointing error, which is 0″.64 at 90% confidence and 1″ at 99% confidence.
[d] The hardness is given by $(C_2 - C_1)/(C_2 + C_1)$, where C_2 is the number of counts in the 2–10 keV band and C_1 is the number of counts in the 0.3–2 keV band.

2–10 keV X-ray fluxes. We have identified IGR J15293–5609 (6) as a likely symbiotic binary with an early K-type giant donor and a white dwarf accretor. For 5a, 7, 10a, and 10b, higher angular resolution or deeper images are necessary to obtain optical/IR counterparts. For 4a, 4b, 5b, and 11, optical or near-IR spectra of the counterparts identified in this work are likely to lead to a determination of the source type.

J.A.T. and A.B. acknowledge partial support from NASA through *Chandra* Award Number GO1-12046X issued by the Chandra X-ray Observatory Center, which is operated by the Smithsonian Astrophysical Observatory under NASA contract NAS8-03060. We acknowledge useful comments from an anonymous referee. This research has made use of the IGR Sources page maintained by J. Rodriguez and A. Bodaghee (http://irfu.cea.fr/Sap/IGR-Sources), the VizieR catalog access tool and the SIMBAD database, which are both operated at CDS, Strasbourg, France. We also acknowledge the use of the 2MASS, USNO, DENIS, and *WISE* catalogs.

APPENDIX

IGR J04069+5042, IGR J06552–1146, IGR J21188+4901, and IGR J22014+6034 are the cases where the candidate counterparts did not clearly stand out from the general population of X-ray sources. However, it is still possible that one of the detected *Chandra* sources is the correct counterpart, and we provide the full lists of sources detected within the ACIS-I fields of view using `wavdetect` in Tables 8, 9, 10, and 11. The ACIS counts reported in the tables are for the full 0.3–10 keV energy band, and we used the same methods described in Section 3.1 to determine the source apertures and the background regions. For each `wavdetect` source, we used Poisson statistics to determine the detection significance, and we did not include sources with significances lower than $\sim 1.2\sigma$. Using simulations, Hong et al. (2005) determined an empirical formula for determining *Chandra* position uncertainties that depends on the number of counts detected and the off-axis angle. For each source, we include the 95% confidence position uncertainties calculated using Equation (5) of Hong et al. (2005). The hardness ratios are also included in the tables for sources with five counts or more. We obtained optical observations of some of the *Chandra* sources in these fields, and the results will be presented in M. Özbey Arabacı et al. (2012, to be submitted).

REFERENCES

Anders, E., & Grevesse, N. 1989, Geochim. Cosmochim. Acta, 53, 197
Balucinska-Church, M., & McCammon, D. 1992, ApJ, 400, 699
Bikmaev, I., Irtuganov, E., Sakhibullin, N., et al. 2010, ATel, 3072
Bird, A. J., Bazzano, A., Bassani, L., et al. 2010, ApJS, 186, 1
Butler, S. C., Tomsick, J. A., Chaty, S., et al. 2009, ApJ, 698, 502
Cardelli, J. A., Clayton, G. C., & Mathis, J. S. 1989, ApJ, 345, 245
Chaty, S., & Rahoui, F. 2012, ApJ, 751, 150
Chaty, S., Rahoui, F., Foellmi, C., et al. 2008, A&A, 484, 783
Cox, A. N. (ed.) 2000, Allen's Astrophysical Quantities (4th ed.; New York: AIP Press)
Cutri, R. M., Skrutskie, M. F., van Dyk, S., et al. 2003, 2MASS All Sky Catalog of Point Sources (NASA/IPAC Infrared Science Archive)
Cutri, R. M., Wright, E. L., Conrow, T., et al. 2011, Explanatory Supplement to the WISE Preliminary Data Release Products, Technical Report
Davis, J. E. 2001, ApJ, 562, 575
Elvis, M., Wilkes, B. J., McDowell, J. C., et al. 1994, ApJS, 95, 1
Filliatre, P., & Chaty, S. 2004, ApJ, 616, 469
Fresneau, A., Vaughan, A. E., & Argyle, R. W. 2007, VizieR Online Data Catalog, 346, 91221
Garmire, G. P., Bautz, M. W., Ford, P. G., Nousek, J. A., & Ricker, G. R. 2003, Proc. SPIE, 4851, 28
Gehrels, N. 1986, ApJ, 303, 336
Güver, T., & Özel, F. 2009, MNRAS, 400, 2050
Hands, A. D. P., Warwick, R. S., Watson, M. G., & Helfand, D. J. 2004, MNRAS, 351, 31
Hong, J., van den Berg, M., Schlegel, E. M., et al. 2005, ApJ, 635, 907
Kalberla, P. M. W., Burton, W. B., Hartmann, D., et al. 2005, A&A, 440, 775
Kennea, J. A., Mukai, K., Sokoloski, J. L., et al. 2009, ApJ, 701, 1992
Kim, M., Wilkes, B. J., Kim, D.-W., et al. 2007, ApJ, 659, 29
Landi, R., Bassani, L., Parisi, P., et al. 2010a, ATel, 2853
Landi, R., Maiorano, E., Fiocchi, M., et al. 2010b, ATel, 2731
Landi, R., Malizia, A., Bazzano, A., et al. 2011, ATel, 3178
Landi, R., Masetti, N., Bazzano, A., et al. 2010c, ATel, 3065
Landolt, A. U. 1992, AJ, 104, 340
Lasker, B. M., Lattanzi, M. G., McLean, B. J., et al. 2008, AJ, 136, 735
Lasker, B. M., Russell, J. L., Jenkner, H., et al. 1996, VizieR Online Data Catalog, 1220
Maiorano, E., Landi, R., Stephen, J. B., et al. 2011, MNRAS, 416, 531
Martini, P., Stoll, R., Derwent, M. A., et al. 2011, PASP, 123, 187
Masetti, N., Parisi, P., Palazzi, E., et al. 2009, A&A, 495, 121
Masetti, N., Parisi, P., Palazzi, E., et al. 2010, A&A, 519, A96
Massaro, F., Paggi, A., D'Abrusco, R., & Tosti, G. 2012, ApJ, 750, L35
Matt, G., & Guainazzi, M. 2003, MNRAS, 341, L13
Monet, D. G. 1998, BAAS, 30, 1427
Monet, D. G., Levine, S. E., Canzian, B., et al. 2003, AJ, 125, 984
Murphy, T., Mauch, T., Green, A., et al. 2007, MNRAS, 382, 382
Negueruela, I., Smith, D. M., Reig, P., Chaty, S., & Torrejón, J. M. 2006, in The X-ray Universe 2005, ed. A. Wilson (ESA SP-604; Noordwijk: ESA), 165
Pellizza, L. J., Chaty, S., & Negueruela, I. 2006, A&A, 455, 653
Ratti, E. M., Bassa, C. G., Torres, M. A. P., et al. 2010, MNRAS, 408, 1866
Smith, D. M., Heindl, W. A., Markwardt, C. B., et al. 2006, ApJ, 638, 974
Sugizaki, M., Mitsuda, K., Kaneda, H., et al. 2001, ApJS, 134, 77
Tomsick, J. A., Bodaghee, A., Rodriguez, J., et al. 2012, ApJ, 750, L39
Tomsick, J. A., Chaty, S., Bodaghee, A., & Rodriguez, J. 2011a, ATel, 3342
Tomsick, J. A., Chaty, S., Bodaghee, A., et al. 2011b, ATel, 3293
Tomsick, J. A., Chaty, S., Rodriguez, J., Walter, R., & Kaaret, P. 2008, ApJ, 685, 1143
Tomsick, J. A., Chaty, S., Rodriguez, J., Walter, R., & Kaaret, P. 2009, ApJ, 701, 811
Tomsick, J. A., Chaty, S., Rodriguez, J., et al. 2006, ApJ, 647, 1309
Walter, R., Zurita Heras, J., Bassani, L., et al. 2006, A&A, 453, 133
Watanabe, C., Ohta, K., Akiyama, M., & Ueda, Y. 2004, ApJ, 610, 128
Weisskopf, M. C. 2005, Space Res. Today, 162, 5
Wilms, J., Allen, A., & McCray, R. 2000, ApJ, 542, 914
Woudt, P. A., & Kraan-Korteweg, R. C. 2001, A&A, 380, 441
Zacharias, N., Monet, D. G., Levine, S. E., et al. 2005, VizieR Online Data Catalog, 1297
Zacharias, N., Finch, C., Girard, T., et al. 2009, VizieR Online Data Catalog, 1315
Zurita Heras, J. A., Chaty, S., & Tomsick, J. A. 2009, A&A, 502, 787